Experimental tests for the application of an analytical model for flexible debris flow barrier design

Experimental tests for the application of an analytical model for flexible debris flow barrier design

A.M. Ferrero[2], A. Segalini[1], G. Umili[1]

[1]{Department of Civil, Environmental and Territory Engineering, University of Parma, Italy}

[2]{Department of Earth Sciences, University of Torino, Italy}

Correspondence to: Andrea Segalini (andrea.segalini@unipr.it)

Abstract

The design of flexible barriers against debris flows is a complex procedure because of the large number of parameters involved. In order to face this difficult task, the Authors have developed a simplified approach. The proposed simplified model involves the determination of parameters related to both the mobilized material and the various mechanical portions of the structure. A calibration phase is required to appropriately model the deformation of the net and the load transfer that occurs between the net and the horizontal structural cables. The determination of the parameters required to set up of the analytical model is discussed in the first part of the paper. Tests carried out to calibrate the transfer function that allows the deformation behavior of the barrier to be reproduced using the analytical model are then reported.

Keywords: Debris flow, analytical model, deformable barrier, on-site test

1. Introduction

The catastrophic effect of the propagation of debris flow phenomena in mountainous areas has favored the development of different protection tools; in particular, considerable attention has been dedicated to the development of high strength flexible barriers similar to those already used for protection from rockfalls. Consequently, several experimental and theoretical studies, in particular, have been aimed at developing specific guidelines to provide designers with specific computational tools that are more suitable than those created for rockfalls (Ferrero et al., 2010).

The interaction between flexible barriers and debris flows is very complex, as reported in several papers (Iverson, 1997; Wartmann and Salzmann, 2002; Bugnion and Wendeler, 2010; Bugnion et al., 2011) that have dealt with on-site tests. However, most of these tests on debris flow barriers lack a numerical and/or analytical interpretation of the results. They are very interesting, as far as the description of barrier behavior under the impact of a debris flow (or mud flow) is concerned, but they cannot easily be compared in a quantitative way, since not all the necessary detailed information is available.

As far as the modeling aspects of the design of flexible barriers are concerned, two different possible approaches are available: the energy approach and the force approach. The energy approach (Wartmann and Salzmann, 2002; Rorem et al., 2013; Wendeler et al., 2010) depends on the duration of the impact and the held back mass and the energy of the flow are therefore drastically overestimated for gradual or intermittent filling events. The impact energy is generally used to choose the class of barrier that has to be installed.

Wendeler et al. (2007) suggested a force approach, based on the conservation of momentum, which assumes that the dynamic impact of the debris flow on the barrier can be computed by means of the balancing equations between the momentum flux and the impulse of the resisting

forces. The original impact force becomes a static load as the arrival of a new front imparts an additional dynamic force.

Numerical methods, based on the discrete elements method (Boetticher et al., 2011), which are able to simulate the impact between a fluid and a structure, have also been developed, but the difficulties involved in setting up the model and the time needed to run it limit its applicability. To the Authors' knowledge, no simple models that can account for both the behavior of the flow and the general structural behavior of the flexible barrier are currently available in literature.

The authors have developed a simplified analytical model for the design of flexible barriers (Brighenti et al., 2013): they feel that such a simplification is necessary since any debris flow occurrence involves such a high number of parameters that it would be almost impossible to access each one in detail. Furthermore, it has been observed that a debris flow that occurs at different times at the same location assumes different behaviors and generates different consequences on the structures each time. The application of the proposed analytical model for the analysis of a debris fence should of course be conducted after an accurate study of the debris flow phenomenon propagation, using an appropriate numerical model. Several numerical propagation models have been introduced in literature (Savage, 1989; Hungr, 1995; Rickenman, 1997; Hungr, 2000). Most of these provide the debris flow front velocity and height at a specific location along its path. Those values are equivalent to the bounce height and block velocity of the rockfall models and, like them, are obtained by simplifying the complexity of the debris flow dynamics (changes in density, water content, internal impacts and energy dissipation, etc.) by making several assumptions. The question that arises is: why should one use a detailed numerical model (i.e. FEM or FDM) in order to analyze a complex and strongly non-linear structure (i.e. the debris net) when its input parameters have already been determined roughly? Would it not be better to use a simplified analytical model that provides fast and easily obtainable solutions and then, eventually, apply some parametrical analysis to the results, in

order to infer the load combination and effect that would most likely occur? In the authors' experience, in Italy, such debris flow nets have been introduced with very few, if any, analytical or numerical verifications, relying mostly on the experience of the producers of such barriers. The idea of proposing a simplified analytical model for the analysis of debris flow protection nets is therefore aimed at providing the scientific community, and the professionals involved in the design of such structures, with an instrument that would allow quick access to the structure performances with an appropriate degree of confidence. The simplifications and assumptions made in the development of the analytical model were introduced for this purpose. The obtained results should, in general, be tested and verified by means of field experiments, such as the one presented below. Data relating to both the flow and the barrier were obviously required in the model: while the flow data refer to the physical and mechanical parameters of the classical soil mechanics or hydraulics, it was necessary, for the data concerning the barrier structure, to prepare specific tests, described hereinafter, which can be classified in two categories:

1. tests for the determination of the barrier deformation characteristics;
2. simulation tests of the debris impact phenomenon, associated to the measurement of the barrier deformation and of the state of stress induced in the various parts of the structure.

The importance of accessing the evolution of the structure deformation during the impact phase made it necessary to apply advanced measurement techniques, and in particular, the application of digital photogrammetry.

2. The Analytical Model

The complete description of the model (Brighenti et al., 2013) is beyond the scope of this paper, consequently a concise description is given hereafter, with identification of the relevant parameters that have to be experimentally determined and the hypotheses that have been made.

The typical barrier for a channelized debris flow has an almost trapezoidal shape and is anchored to the ground (generally at the channel sides) by means of grouted anchors or cables. The main structural cables are horizontal and their number depends on the overall height and on the expected flow characteristics. The barrier net consists of two meshes: the main one, formed by larger rings, is suitable for holding the larger size material and gives the structure its strength, while the latter, which consists of smaller hexagonal elements, is suitable for containing also fine grain material, even though it does not contribute to the strength of the structure. The model assumptions and their justifications are given hereafter.

The introduced model considers that the main resisting cables are loaded, only in a horizontal plane, by the forces produced by both the static load and the debris impact on the barrier, while the resultant of the vertical forces transmitted by the connecting net to each single cable is considered negligible. As a consequence, only the deformation of the cables in the horizontal plane are assumed to be significant in the resistant mechanism of the structure.

It should also be considered that the vertical components of the forces acting along a single cable are only significant for the uppermost one, since the lower and the intermediate cables of the barrier are usually either restrained by the channel bottom or symmetrically surrounded by other cables, and, as a consequence, they are subjected to a simple, almost horizontal force. Moreover, the vertical components of the load are generally not negligible, in terms of absolute values of the forces generated within the structural cables. However, in relative terms, the impact pressure is parallel to the debris flow direction on impact and, although at first it is directed parallel to the slope, it rapidly changes in direction once the debris starts to pile up behind the barrier, becoming approximately horizontal. The steeper the slope behind the barrier, the faster the debris piles up and creates an almost horizontal ramp for the incoming flow. When the active flow hits the highest portion of the barrier, the barrier pocket at the bottom is only subjected to static pressure, which is always considerably lower than the pressure induced on

the same portion of the net by the direct impact of the flowing material (proportional to the square of its velocity).

While calculating the pressure acting on the barrier, the model does not take into account the deformation induced in the net by the pressure exerted by the flowing granular material; since the case of a rigid barrier is the most critical in the design of such retention structures, the mitigation of the pressure, due to the net deformation, can reasonably be neglected from the safety point of view. This hypothesis holds true since the maximum transversal displacement of the barrier, inferred from both experimental and numerical results, is usually much lower (10–15%) than the barrier extension.

The assumption of a constant load along the cable is an acceptable simplification from the engineering safety point of view; this hypothesis allows one to treat the problem as a two dimensional one, characterized by governing equations that can easily be handled for a simplified design of the retention barrier, as will be shown hereafter.

A further assumption concerns the dissipating elements that are considered in the model, since the presence of these devices (often referred to as brakes) in debris flow net barriers is quite common; such devices operate by dissipating energy and increasing the cable length once the maximum allowable force of the brake is reached. The brakes are considered in the calculation using an iterative procedure; once the axial load on one structural cable equals the activation force, the brake is elongated by a small amount (1/10-1/100 of its original length) and then the load on the cable is recalculated. If it is now lower than the activation force, the calculation proceeds, otherwise another small elongation is made and the iteration continues until the brake has reached its maximum length.

From this point onward the cable behaves exactly like it did before activation of the brake, but with its length increased. This increased length produces a beneficial effect as it induces a

decrease in the tension forces in the cables, although neglecting the brakes usually leads to a conservative design of the barriers.

By considering the barrier made of *n* cables at a relative distance equal to *p* (Fig. 1), the total horizontal load $q(z_i,t)$ acting on the i-th cable located at the vertical coordinate $z_i, \geq h_0$ can simply be calculated by means of Eq. (1):

$$q(z_i \geq h_0, t) = \begin{cases} 0 & t < t_1 = (z_i - h_0)^2/(2 \cdot v_0 \cdot h_0 \cdot tan\theta) \\ q_d = \alpha \cdot \rho_d \cdot v_0^2 & t_1 \leq t \leq t_2 = z_i^2/(2 \cdot v_0 \cdot h_0 \cdot tan\theta) \\ q_s = k \cdot \left[h_0 + h(t) - h_B \cdot \frac{(i-1)}{(n-1)}\right] \cdot \rho_d \cdot g & t > t_2 \end{cases} \quad (1)$$

while Eq. (2) should be used when the i-th cable is located at vertical coordinate $z_i < h_0$:

$$q(z_i < h_0, t) = \begin{cases} q_d = \alpha \cdot \rho_d \cdot v_0^2 & t < t_1 = z_i^2/(2 \cdot v_0 \cdot h_0 \cdot tan\theta) \\ q_s = k \cdot \left[h_0 + h(t) - h_B \cdot \frac{(i-1)}{(n-1)}\right] \cdot \rho_d \cdot g & t \geq t_1 \end{cases} \quad (2)$$

where h_0 is the constant height of the debris flow surge.

Figure 1. Debris accumulation behind the barrier and the corresponding loads at different time steps: (a) t=0, (b) t>0 (Brighenti et al., 2013)

The governing equation of the equilibrium of a loaded cable can usefully be employed to describe the mechanical behavior of such a structural system. Let us consider the barrier constituted by several horizontal cables mounted at a reciprocal constant distance of *p* (Fig. 2a). The i-th cable - having its extremities fixed at points A and B - is characterized by an effective length L_i and a projected length l_i along the x-axes (Fig. 2b). The distributed load acting on such a cable is assumed to lie in a horizontal plane and to be constant with respect to the *x* coordinate at a fixed time *t*. The load, however, is variable with time, since the depth *d(t)* of the cable, with respect to the top surface of the flowing material, increases with *t* (Fig. 1b).

Figure 2. a) Scheme of cables forming a barrier and of the forces developed in cable j for a load acting on cable i; b) scheme of a single cable under the forces produced by the impact of a debris-flow (Brighenti et al., 2013)

Since the horizontal cables are connected by the barrier net, it can be assumed that they are joined together by 'equivalent' vertical cables that have the effect of distributing a portion of the load applied directly to each horizontal cable to the adjacent ones (Fig. 2a). By indicating with $\bar{u}_{ij}$ the maximum displacement that occurs in cable j when cable i shows a maximum displacement equal to $\bar{u}_i$, an influence function $0 \leq r(z_j, z_i) \leq 1$ can be written in order to correlate the above quantities:

$$\bar{u}_{ij} = r\left(z_j, z_i\right) \cdot \bar{u}_i \tag{3}$$

The value of the distributed ''indirect'' load q_{ij} (Fig. 2a), acting along a generic cable j transmitted from cable i, can be expressed as:

$$q_{ij} = q_i \cdot \frac{r^3\left(z_j, z_i\right) \cdot C_j}{\sum_{k=1}^{n} r^3\left(z_k, z_i\right) \cdot C_k} \tag{4}$$

with

$$C_j = \frac{64 \cdot E_j \cdot A_j}{3 \cdot l_j^4} \tag{5}$$

and

$$C_k = \frac{64 \cdot E_k \cdot A_k}{3 \cdot l_k^4} \tag{6}$$

The above introduced function $r(z_j, z_i)$ can reasonably be assumed in the form:

$$r(z_j, z_i) = \frac{1}{\left(|z_j - z_i| + 1\right)^{m_{ji}}} \tag{7}$$

where

$$m_{ji} = \frac{-\ln(c)}{\ln\left(|z^* - z_i| + 1\right)} \tag{8}$$

in which $r(z^*, z_i) = c$ is the value attained by function $r(z_j, z_i)$ at vertical coordinate $z_j = z^*$ (i.e. for a cable placed at a relative distance from cable i equal to $d_{*i} = |z^* - z_i|$), while the unit value of $r(z_j, z_i)$ is attained at $z_j = z_i$ (Fig. 3).

Fig. 3. Assumed pattern of function $r(z_j, z_i)$ for different values of exponent m and for z_i = 4 (Brighenti et al., 2013)

The described mechanical model has been implemented in a simple in-house made Fortran code, and a line command executable software has been generated.

2.1 Required parameters

As already mentioned, the model requires the input of several parameters relative to both the flow and the barrier; these parameters are listed in Tables 1 and 2. This section is reported in order to show that several theories already exist that can be used to describe how the flow velocity and height should be determined at each location along the debris flow path. The results of the different approaches and the assumptions that each approach requires lead to a range of

solutions and possible conditions that can be applied as input in the simplified model. Therefore, the choices made to develop the analytical model were aimed at providing meaningful results, under a particular impact condition, to be obtained from software for debris flow analysis such as DAN-W (Hungr, 1995) or similar. The assumptions that were introduced into the simplified analytical model are combinations of the most critical conditions (load uniformly distributed along the entire width of the channel) and the feasibility of an analytical solution of a structurally complex construction subjected to spatially and temporally variable loads.

Table 1. Flow parameters

Table 2. Barrier parameters

The flow velocity v_0, needed for a debris flow to transport the load without erosion or deposition, can be calculated as (Takahashi et al., 1992):

$$v_0 = \frac{2}{5D}\left(\frac{g \cdot \sin\theta_e \cdot \rho_d}{0.02 \cdot \sigma}\right)^{1/2} \cdot \frac{1}{\lambda} \cdot h_0^{3/2} \tag{9}$$

where θ_e, which represents the channel slope in which concentration *c* is in equilibrium, can be obtained from:

$$\tan\theta_e = \frac{c \cdot (\sigma - \rho) \cdot \tan\phi}{c \cdot (\sigma - \rho) + \rho} \tag{10}$$

and λ, the linear concentration of the solids in the flow, can be calculated as:

$$\lambda = \left[\left(\frac{c_*}{c}\right)^{1/3} - 1\right]^{-1} \tag{11}$$

The parameters required to calculate the flow velocity with Takahashi's formulation are listed in Table 3.

Table 3. Debris parameters required for the velocity v_0 calculation

Figure 4 shows the velocity variation with flow thickness for different grain dimensions (D), considering Takahashi's formulation, expressed by Eq. (9), and with the values listed in Table 4. Velocity can change remarkably according to the nature of the material and to the flow entity and it is therefore very important to carefully choose the velocity value that has to be assumed in the analytical model.

A comparison of the results from Takahashi's formulation and those obtained with other approaches proposed to estimate the maximum (mean cross-sectional) velocity of the frontal part of debris flows (Rickenmann, 1999; Lo, 2000) is shown in Figure 4. In particular, the following flow models were considered:

- Newtonian laminar flow: $$v_0 = \frac{\rho_d \cdot g \cdot h_0^2 \cdot \tan\theta}{\zeta \cdot \mu_d} \quad (12)$$
- Newtonian turbulent flow: $$v_0 = \frac{1}{n} \cdot h_0^{2/3} \cdot (\tan\theta)^{1/2} \quad (13)$$
- Dilatant flow: $$v_0 = \xi \cdot h_0^{3/2} \cdot (\tan\theta)^{1/2} \quad (14)$$
- Empirical formula: $$v_0 = k^* \cdot h_0^{2/3} \cdot (\tan\theta)^{1/5} \quad (15)$$

with $\zeta = 3$ (corresponding to a wide rectangular channel), $\mu_d = 3\ kPa \cdot s$ (Hungr et al., 1984), $1/n = 28.5 h_0^{-0.34}$(Du et al., 1987), $\xi = 2.17\ m^{-0.5} \cdot s^{-1}$ (Hungr et al., 1984) where k* is a function of h_0 (see Table 5).

Table 4. Parameter values assumed to obtain Figure 4

Table 5. Values of k* in function of h_0

Figure 4. Variation of the debris velocity according to its thickness, using different flow models

2.2 Calibration of function r

In order to appropriately predict the cable deformation, the function $r(z_j, z_i)$, expressed by Eq. (7), needs to be properly tuned through its coefficient m_{ji}, which represents the relation between the displacements of two different cables connected through the barrier net. The authors, using the specific calibration test described hereafter, have determined the coefficient m_{ji}.

2.2.1. Test site

The test site, which is owned by the Consorzio Triveneto Rocciatori, is located in Fonzaso (Belluno, Italy): it consists of a sub-vertical cliff on which a barrier can be installed almost horizontally, that is almost perpendicular to the slope. In particular, the test net is composed of 6 parallel steel cables (20 mm diameter steel cables - UNI EN 12385-4 6x19 Metal Core - Strenght Class 1770 N/mm^2) on which the metal net is connected; the inter-axis between the cables is about 1 m and the cables were pre-tensioned in order to reduce the catenary shape induced by the self-weight of the barrier. The main metal net is made up of interweaved steel wire that forms 0.35 m diameter rings. The steel wire is characterized by a diameter of 3 mm and by a strength class of 380-550 N/mm².

The barrier used for this calibration is a part of an experimental prototype developed by Consorzio Triveneto Rocciatori S.c.a.r.l., called CTR mod. RMC 100/DF 2-4. The opposite ends of the barrier cables are fixed to parallel beams mounted perpendicular to the cliff face at a distance of 10 m.

Digital images of the tested barrier are taken using two fixed high resolution digital cameras (Fig. 5). Before the test, 14 Ground Control Points (GCP) were materialized by sticking 14 targets onto the rock. Moreover, another 10 easily recognizable natural points were chosen over the rock outcrop. A total of 24 GCP coordinate sets (XYZ) were obtained by means of the photogrammetric restitution. A reference distance was used to scale the model. A photogrammetric survey of the barrier was then carried out at the test site, in order to define a single reference system for the whole test procedure and to acquire the referred GCP coordinates. A sequence of 6 photographs was taken with a Nikon D3X camera, on which a calibrated 18 mm lens was mounted.

Figure 5: scheme of the test site and the barrier: side view

A photogrammetric acquisition system was then set up: two high-definition digital cameras, each fixed onto a tripod, were located so that each field of view included the entire barrier. Camera 1 is a Nikon D3X with the 18 mm lens mentioned above, while camera 2 is a Canon EOS 5D with a calibrated 20 mm lens. The first and the second images of a stereo pair are obtained from Camera 1 and Camera 2, respectively. The stereo pairs obtained by these cameras in each test were used to establish the barrier geometry. The aim of the tests was to obtain the geometry of the barrier under different loading conditions. Four different load combinations were applied (Fig. 6) and considered for each cable:

- Combination 0: no loads;
- Combination 1: 9 identical loads of 0.7 kN distributed along each single cable, no loads on the other 5 cables;
- Combination 2: 9 identical loads of 1.4 kN distributed along each single cable, no loads on the other 5 cables;
- Combination 3: a single load of 16.16 kN applied in the middle of each single cable, no loads on the other 5 cables.

Combination 0 refers to the unloaded situation: the stereo pairs were acquired to reconstruct the original barrier geometry, in order to perform comparisons later on with the barrier deformed by each load. Combination 1 was then applied to cable 1 of the barrier by fixing the 9 loads along cable 1; the same Combination 1 was then applied to the other cables, by simply transferring the applied loads. A total of 6 stereo pairs, one corresponding to each loaded cable, was obtained. An identical procedure was carried out for load Combination 2, and another 6 stereo pairs were obtained. The same was done for load Combination 3. The expected accuracies, calculated considering the normal case of terrestrial photogrammetry (Kraus, 2007), are listed in Table 6.

Figure 6: a) Scheme of load combinations 1 and 2; b) load combination 3

Table 6: expected accuracy of the barrier point coordinates

Owing to the fixed camera assets, the exterior orientation parameters of images 1 and 2 of each test do not change from one stereo pair to another. This is a great advantage, because no errors are introduced due to exterior orientations. All the images were processed to remove radial and tangential distortion; then, by means of a monoscopic digital restitutor, each of the 19 stereo pairs was oriented and georeferenced using at least 11 GCPs, out of the 24 materialized ones.

Fifty-four points, homogeneously distributed along the cables, were collimated (Fig. 7) on the stereo pair representing the undeformed condition (Combination 0) and their X,Y and Z coordinates were obtained by means of photogrammetric restitution. The accuracy ranges of the barrier point coordinates, expressed by their standard deviations, are listed in Table 7: these ranges were automatically calculated by the restitutor through a bundle adjustment, that is, a complex algorithm that optimizes all the available data to indicate the best positions and angles of the camera at the time of exposure and the positions of the 3D data points. The values of σ_y and σ_z were greater than the expected accuracies (Table 6), but acceptable for the aim of the work, that is, the reconstruction of the shape of the deformed barrier, rather than the measurement of the deformation itself. The same 54 points were then collimated on all the other 18 stereo pairs; however, in 11 of the 18 stereo pairs, 2÷6 of these points were hidden by the loads fixed to the cables, and, as a result, they could not be restituted. However, this fact did not compromise the global deformation reconstruction.

Figure 7: 54 surveyed points on the barrier

Table 7: obtained accuracy of the barrier point coordinates

2.2.2. Calibration procedure

The Genetic Algorithm (GA) (Goldberg, 1989; Gen and Cheng,1996) that is used to obtain the proper exponent m_{ij} - necessary for the definition of the interaction function between each couple of cables i, j, $0 \le r(z_j, z_i) \le 1$ - has been applied for each loaded cable, as shown in Figure 8. The exponents m_{ij}, collected in a square, non symmetrical matrix, are characteristics of the particular barrier tested and are used for the subsequent calculation of the mechanical response of the barrier against the debris flow phenomenon.

Figure 8. Comparison of experimental data and numerical results after calibration of the parameters involved in the interaction function, $0 \le r(z_j, z_i) \le 1$, between cables

It can in fact be noted that the exponents m_{ij} and m_{ji} related to the cable couple i, j , are generally different from each other. This occurs since the displacements that arise in cable *i*, when cable *j* is displaced by a certain amount, are in general different from those that arise in cable *j* when cable *i* is displaced, because of the non-linearity characteristic of the system of governing equations (Brighenti et al., 2013). The 'conventional' cross section area of the transversal cables (secondary cables), which are used to simulate the metallic net connecting the horizontal cables (main ones), must be set on the basis of the experimental data measured on the real barrier described in the previous section and considering the previously determined m_{ij} exponents determined. Therefore, a least square algorithm can be used to obtain the optimum value of such a quantity. Four cases are presented in Figure 8: cables No.s 2, 3, 4 and 5 are displaced by applying a distributed load to each, and the maximum displacements that arise in all the remaining main cables are measured and reported as dots. The simulation results, obtained through the above explained procedure using the best choice of exponents m_{ij} and the optimum value of the cross-section area of the secondary cables, are shown with continuous lines. The agreement between the experimental and numerical data is quite satisfactory, both in terms of displacement values and the deformed pattern of the cable in the mid-section of the barrier. It is apparent that the assumption of the interaction function (see Eq. (7)), proposed in Brighenti et al. (2013), is suitable for the numerical simulation of the cable interaction, once its governing parameters have been properly determined. No force sensors were required for the first test (calibration of m_{ji}), since predefined weights were applied directly to the structures in order to simulate a particular load combination. Either the force or the position of each applied

weight was known and the forces developed inside each cable were calculated using an analytical solution (cable loaded in the vertical deformation plane). The only measured entities for this test were the deformations of the cables induced by the load acting on the other cables. The test set up can easily be reproduced at one of the test sites recently developed and used for rockfall barrier certification according to ETAG 027. Authors chose to operate as described in order to allow any barrier producer to repeat this calibration test, with limited economic and technical efforts, for each model or to configure a debris flow barrier kit. The main objective of this study was to develop a standard procedure that would allow each debris flow barrier kit to be quantified in a similar way to those developed in the EU for the certification of rockfall barrier kits (ETAG027).

3. In situ full size test

A full-size test of a debris flow impacting a flexible barrier has been carried out at Pieve di Alpago (Belluno, Italy), using an appropriately built barrier, in order to obtain results for comparison with those calculated using the analytical model. The test was carried out according to the following steps:

1) Site preparation: a 43m long, 2m wide channel and with an almost constant trapezoidal section was artificially profiled with a slope of about 40 degrees.
2) Debris preparation: loose limestone material obtained from the quarry, characterized by a variable diameter size of between 0.1÷1.5 m and by an average density, estimated on impact with the structure, of 1790 kg/m^3, was used. The material was initially stored in the upper part of the channel. The total volume of the used material was approximately 400 m^3.
3) A topographic survey of the site was carried out using a Total Station: first, a local reference system was fixed; then 14 Ground Control Points (GCPs) were materialized after driving

colored nails into the rock, and their coordinates were measured in order to geo-reference the images later on. Finally, a point cloud of the channel was acquired. The Digital Surface Model (DSM), which was created triangulating the point cloud, was composed of 15760 points, and had a density of 10÷15 pts/m^2.

4) The barrier, which was instrumented with 5 load cells, was installed at the bottom of the channel, to stop the mobilized material. Two high-definition video cameras (23 fps frame rate) were placed in front of the barrier, to create a stereoscopic configuration, in order to obtain the 3D deformation of the barrier during the test.
5) The test was carried out: the debris, previously stored near the upper part of the channel, was released from the top of the channel from trucks; this caused the formation of several surges with similar flow rates at the beginning of the channel. The impact force was evaluated during the test, by monitoring the load cell data and checking the behavior of the brakes.
6) A new topographic survey of the site was carried out in order to compare the pre and post-test conditions.

3.1. Barrier

The barrier was placed downstream from the channel: it was fixed on three sides (left, bottom, right) by means of anchors and nails driven into the rock. The barrier was composed of five horizontal bearing elements (with two cables each) and two superimposed metal meshes. The cables that made up the horizontal bearing elements were 20 mm diameter iron cables (UNI EN 12385-4 6x19 Metal Core - Strength Class 1770 N/mm^2). The upper bearing element corresponded to the upper boundary of the barrier; the other four bearing elements were parallel to each other (inter-axis is about 1.3 m) and each cable of the element was equipped with two

special brakes designed to dissipate the impact energy. The brakes, 600 mm in length, dissipated energy through the deformation of the coating material, which consisted of Ø 3 mm Al 6060 aluminum tubes with a thickness of 1.5 mm. They were equipped, at both ends, with aluminum buffers and sleeves, which acted as stroke ends and were constructed according to the UNI EN 13411-3 Standard. The activating force of each break was 60 kN and their total elongated length was 1 m. The primary net was composed of circular rings (diameter 0.35 m), while the second was formed by hexagonal elements (diameter of the inscribed circle 0.08 m). The steel wire was characterized by a diameter of 3 mm and by a strength class of 380-550 N/mm². The barrier used for the test was an experimental prototype developed by Consorzio Triveneto Rocciatori S.c.a.r.l., called CTR mod. RMC 100/DF 2-4. The barrier had a trapezoidal shape and its dimensions are reported in Table 8, in which the characteristics of the cables are also reported, according to the UNI EN 12385-4 Standard, together with the characteristics of the principal mesh, according to the same Standard.

Table 8. Characteristics of the barrier, cables and principal mesh (according to the UNI EN 12385-4 Standard)

3.2. Monitoring system

The aim of the implemented monitoring system was to obtain two different kinds of data: impact forces and barrier deformations. Although the forces were registered directly by the load cells, the deformations were not measured directly on the barrier, because interest was focused on the global deformations: a DSM of the whole net was therefore required. A photogrammetric acquisition system was created: two identical, previously calibrated video cameras, *Basler Pyton GigE*, were fixed to a metal bar, at a distance of 2.7 m; they were positioned in front of

the net barrier, at a distance of 14 m from the center, so that the whole barrier was completely visible in the field of view of both cameras. The two cameras filmed continuously during the test (duration 1200 seconds), with a synchronized video frequency of 23 fps; therefore, a total of 27600 stereo pairs were available. Owing to the fixed camera assets, the exterior orientation parameters of images 1 and 2 did not change from one stereo pair to another, and, therefore, no errors due to exterior orientation were introduced. The stereo pair obtained just before the test was started (S_0) was processed to remove radial and tangential distortion; then, by means of a monoscopic digital restitutor, 69 points, homogeneously distributed over the barrier, were collimated on both stereo pair images. Moreover, 11 GCPs, out of the 14 materialized, were used to georeference the block (Fig. 9).

Figure 9: S_0 stereo pair processed by means of monoscopic digital restitution

The accuracy ranges of the barrier point coordinates, expressed by their standard deviations, are listed in Table 9: they were automatically calculated by the digital restitutor through a bundle adjustment.

Table 9: obtained accuracy of the barrier point coordinates

It is possible to observe that the calculated accuracies are smaller than the expected accuracies: this proves that the errors introduced by the GCP coordinates and the point collimations had been taken into account correctly. Therefore, the implemented monitoring system can be considered stable and reliable. After the test was started, 6 significant instants (S_1, S_2, S_3, S_4, S_5, S_6) were chosen, and the relative stereo pairs were processed in the same way as described

for the S_0 stereo pair. The same points and GCPs materialized in S_0 were collimated in each stereo pair. Only 60, out of the 69 original points, were visible in all the 7 stereo pairs: 9 points in the lower part of the barrier were lost, due to the large deformation caused by the debris accumulation. At the end of the photogrammetric restitution, the X,Y and Z coordinates of each point on the barrier were known at the 7 considered instants, thus allowing the barrier deformations to be checked. After the six stereo pairs had been processed and the correspondent DSMs had been created, barrier deformation was checked in the mid-section.

Five out of eight anchor points were equipped with 1000 kN load cells and were connected to a data logger that recorded the traction force in each cable at a rate of 100 Hz.

The registered flow velocity, on average, was 2.51 m/s with measured peaks of 9 m/s. The total volume stopped at the barrier was approximately 400 m^3: two laser scanner surveys were performed before and after the test, respectively, so that the two DSMs could be compared in order to obtain the volume of the amassed material. The average flow height, $h_{0,}$ was equal to 0.7 m, while the material density was estimated as 1790 kg/m^3. The test came to an end when the whole barrier was filled; no overflow was allowed for test site safety reasons.

3.3. Comparison between the analytical model and the in situ test

The analytical model has been solved to describe the loads hitting on the barrier. The values of the empirical coefficient α and of the earth pressure coefficient k were determined through back-analysis, considering the indications of Canelli et al. (2012) and Bugnion et al. (2012). The exponent m_{ji} of functions $r(z_j, z_i)$ which relates each cable to the others – i.e. for the assessment of the cable interaction – was calculated according to the GA procedure described in Brighenti et al. (2013).

Table 10. Parameter values used to simulate the in situ test

Figure 10. Vertical sections at the midspan length position of the retention barrier during the loading process: experimental results for the on-site tests carried out at the Pieve di Alpago (Belluno, Italy) site (a) and corresponding numerical results (b). The cross and square symbols indicate the initial and final deformed shape of the barrier, respectively.

A comparison between the experimental and numerical results is shown in Figure 10 in terms of deformation of the retention barrier during loading. A comparison between the induced tensions in the cable net in time is shown in Figure 11. Although some differences between the experimental and numerical results were recorded, especially concerning the barrier deformation, the induced states of traction in the cables were in good agreement. This is possibly due to an unknown initial state of stress in the cables induced during the structure assembly; this initial state of stress did not influence the cable tensions induced by the flow, but only their deformations, mostly in the starting phases and in the upper part of the loading process. The lower part of the net slides in the model, while it is fixed on-site.

Figure 11. Tension forces in the horizontal cables during the loading process: the experimental results for the on-site tests carried out at Pieve di Alpago (Belluno, Italy) and the corresponding numerical results are reported.

Figure 12. Deformed patterns obtained from the presented model for t=0.5 s (a), t=2.5 s (b) and t=5.0 s (c) (see Figs. 10, 11), corresponding to the simulation of the on-site tests described above.

A full 3D reconstruction of the net during loading is also given in Figure 12: this shows how the method can realistically reproduce the net evolution in time. This kind of result could be usefully applied in the future to set up real time net monitoring systems. In fact, since a continuous monitoring of a channel would require a large amount of space for data storage, a system that is able to activate the monitoring operations through sensors could improve the efficiency of the monitoring to a great extend, and, for this reason, threshold activation values should be defined. The results obtained from the proposed analytical model, in terms of time, could support the correct choice and the set-up of time resolution and instrumentation typology.

4. Conclusions

Debris flow phenomena are often very destructive and dangerous: the design of retention devices, either in populated areas or where it is necessary to limit the destructive effects of these phenomena, is currently limited to simplified approaches. However, the FEM modeling of these kinds of structures, coupled to debris flow impact dynamics, is very difficult due to the non-linearity of the structure, and it is not always practical in real cases. A simplified structural model of cable-like retention barriers has been developed for the aforementioned reasons; in this paper, the analytical model is recalled briefly and the calibration procedure of the function used to predict cable deformations is explained. The main assumptions of the model are that the vertical load and the barrier deformation are neglected. All the assumptions are conservative, from the safety point of view and, moreover, the comparison between the

experimental and theoretical results is satisfactory, although some differences have been observed due to the differences in both the initial experimental conditions and the theoretical boundaries. This model can therefore be considered a useful tool for parametric analyses, which are always suggested when dealing with natural phenomena when a large variability of the ruling parameters is expected. The obtained results could also be used to set up real time monitoring systems.

5. Acknowledgments

A part of this research was carried out with the financial Support of the Italian Ministry of Economic Development. The Authors wish to acknowledge the Consorzio Triveneto Rocciatori S.C.a.r.l. and the Officine Maccaferri S.p.a. for their substantial support in the development of this work.

References

Brighenti, R., Ferrero, A.M., Segalini, A., 2013. Debris flow hazard mitigation: a simplified analytical model for the design of flexible barriers. Comp. Geotech. 54, 1-15.

Boetticher, A.V., Hübl J., Wendeler, C., Volkwein, A., 2011a. Modeling the impact of shallow landslides on flexible protection barriers. Math. Geosci. Crossroads Theory Pract. Marschallinger, R. & Zobl, F., Salzburg, Austria, pp 659–670.

Bugnion, L., Wendeler, C., 2010. Shallow landslide full-scale experiments in combination with testing of a flexible barrier. In: De Wrachien D, Brebbia CA (eds) Monit. Simul. Prev. Remediat. Dense Debris Flows III. WIT Press, Ashurst, Southampton, UK, pp 161–173.

Bugnion, L., McArdell, B.W., Bartelt, P., Wendeler, C.., 2012. Measurements of hillslope debris flow impact pressure on obstacles. Landslides 9(2), 179-187.

Canelli, L., Ferrero, A.M., Migliazza, M.R., Segalini, A., 2012. Debris flow risk mitigation by the means of rigid and flexible barriers – experimental tests and impact analysis. Nat. Hazards Earth Syst. Sci. 12, 1693–1699.

Du, R., Kang, Z., Chen, X., Zhu, P., 1987. A comprehensive investigation and control planning for debris flow in the Xiaojiang river basin of Yunnan province. Science Press, 287 pages (in Chinese).

Ferrero, A.M., Giani, G.P., Segalini, A., 2010. Numerical and experimental analysis of debris flow protection fence efficiency. Rock Mechanics in Civil and Environmental Engineering - Proceedings of the European Rock Mechanics Symposium, EUROCK 2010, pp. 575-578.

Ferrero, A.M., Migliazza, M.R., Roncella, R., Segalini, A., 2011. Rock cliffs hazard analysis based on remote geostructural surveys: The Campione del Garda case study (Lake Garda, Northern Italy). Geomorphology 125, 457-471, ISSN: 0169-555X, doi: 10.1016/j.geomorph.2010.10.009.

Gen, M., Cheng, R., 1996. Genetic algorithms and engineering design. 1st ed. New York: John Wiley and Sons, 40.

Goldberg, D.E., 1989. Genetic algorithms in search, optimization, and machine learning. MA: Addison-Wesley Publishing Company Inc: pp. 1–56.

Hungr, O., 1995. A model for the runout analysis of rapid flow slides, debris flows and avalanches. Can. Geotech. J., 32, 610 - 623.

Hungr, O., Morgan, G.C., Kellerhals, R., 1984. Quantitative analysis of debris torrent hazards for design of remedial measures, Can. Geotech. J. 21, 663–677.

Hungr, O., 2000. Analysis of Debris Flow surges using the theory of uniformly progressive flow. Earth Surf. Proc. Landforms 25, 483-495.

Iverson, R.M., 1997. The physics of debris flows. Rev. Geophys. 35, 245–296.

Kraus, K., 2007. Photogrammetry: Geometry from Images and Laser Scans, Volume 1. Walter de Gruyter, 459 pages.

Lo, D.O.K., 2000. Review of natural terrain landslide debris-resisting barrier design. Geotechnical Engineering Office Report No. 104. The Government of Hong Kong Special Administrative Region.

Rickenman, D., 1999. Empirical Relationships for Debris Flows. Nat. Hazards 19, 47–77.

Rickenman, D., Koch, T., 1997. Comparison of debris flow modelling approaches. Proceedings of First International Conference on Debris-Flow Hazards Mitigation. ASCE: San Francisco, pp. 576-585.

Rorem, E., Wendeler, C., Roth, A., 2013. Flexible debris flow barriers in fire burned areas. In: Margottini C, Canuti P, Sassa K (eds) Landslide Sci. Pract. Springer, Rome, pp 227–232.

Savage, S. B., Hutter, K., 1989. The motion of a finite mass of granular material down a rough incline. J. .Fluid Mech. 199, 177-215.

Takahashi, T., Nakagawa, H., Harada, T., Yamashiki, Y., 1992. Routing Debris Flows With Particle Segregation. J. Hydraul. Eng. 118,1490-1507.

Wartmann, S., Salzmann, H., 2002. Debris flow and floating tree impacts on flexible barriers. Nat. Terrain - Constraint Dev. IMMM Press, Hong Kong, pp 125–132.

Wendeler, C., Balg, C., Singha, G., 2010. Flexible debris flow barriers as hazard mitigation system. Proc. 6th Asian Rock Mech. Symp. New Delhi, India.

Wendeler, C., Volkwein, A., Roth, A., et al., 2007. Field measurements and numerical modelling of flexible debris flow barriers. In: Chen H, Major JJ (eds) Debris-Flow Hazards Mitig. Mech. Predict. Assess. Millpress, Rotterdam, pp 681–687.

Table 1

Click here to download Table: Table 1.docx

v_0	Arrival velocity of the debris flow
h_0	Constant height of the debris flow
k	Coefficient of active earth pressure
ρ_d	Mass density of the debris flow
θ	Inclination angle of the slope
α	Empirical coefficient for dynamic pressure estimation

Table 2

Click here to download Table: Table 2.docx

A	Cross section of the cable
d(t)	Depth of the generic cable measured with respect to the top free surface of the accumulated material
E	Young modulus of the cable
h_B	Total height of the barrier
L_i, l_i	Effective length and projected length along the x-axes of the cable i, respectively
n	Number of horizontal cables in the barrier
p	Vertical distance between the horizontal cables
$r(z, z_i)$	Function defining the horizontal displacement ratio between the cable *i* and the cable plated at the vertical coordinate *z*

Table 3

Click here to download Table: Table 3.docx

D	diameter of the 50% of passing grains
g	Gravitational acceleration
σ	Mass density of solid portion
c_*	Volume concentration of the solids in the static bed
c	Mean volume concentration of the solids throughout the entire flow depth
ϕ	Internal friction angle of the bed
ρ	Mass density of the interstitial water

Table 4

Click here to download Table: Table 4.docx

D	0.02 - 0.06 – 0.6 m
σ	2700 kg/m^3
ρ_d	1790 kg/m^3
θ	40°
h_0	1- 6 m
c_*	0.55
c	0.651
ϕ	30°
ρ	1000 kg/m^3

Table 5

Click here to download Table: Table 5.docx

h_0 (m)	k*
<2.5	10
3	9
4	7
5	5

Table 6

Click here to download Table: Table 6.docx

σ_x [m]	σ_y [m]	σ_z [m]
0.009÷0.010	0.011	0.011

Table 7

Click here to download Table: Table 7.docx

σ_x [m]	σ_y [m]	σ_z [m]
0.007 ÷ 0.009	0.013 ÷ 0.023	0.013 ÷ 0.023

Table 8
Click here to download Table: Table 8.docx

Width at the base (m)	14.85
Width at the maximum height (m)	19.72
Height at the centreline (m)	4.00
Type of cable	Steel, spiral
Diameter (mm)	20
Formation	6×19+AM
Strength class (N/mm²)	1770
Ultimate tensile strength (kN)	252
Type of rings	ASM 3-4-350/500 concatenated with 4 contact points, consisting of galvanized steel wire which form 10 spires
Ring nominal diameter (mm)	350
Steel wires diameter (mm)	3
Wire strength class (N/mm²)	1380
Ultimate tensile strength (kN)	9.5

Table 9

Click here to download Table: Table 9.docx

σ_x [m]	σ_y [m]	σ_z [m]
0.004 ÷ 0.025	0.004 ÷ 0.028	0.003 ÷ 0.008

Table 10

Click here to download Table: Table 10.docx

v_0	2 m/s
h_0	0.7 m
k	0.5
ρ_d	1790 kg/m^3
θ	40°
α	1.5

Figure 8a
Click here to download high resolution image

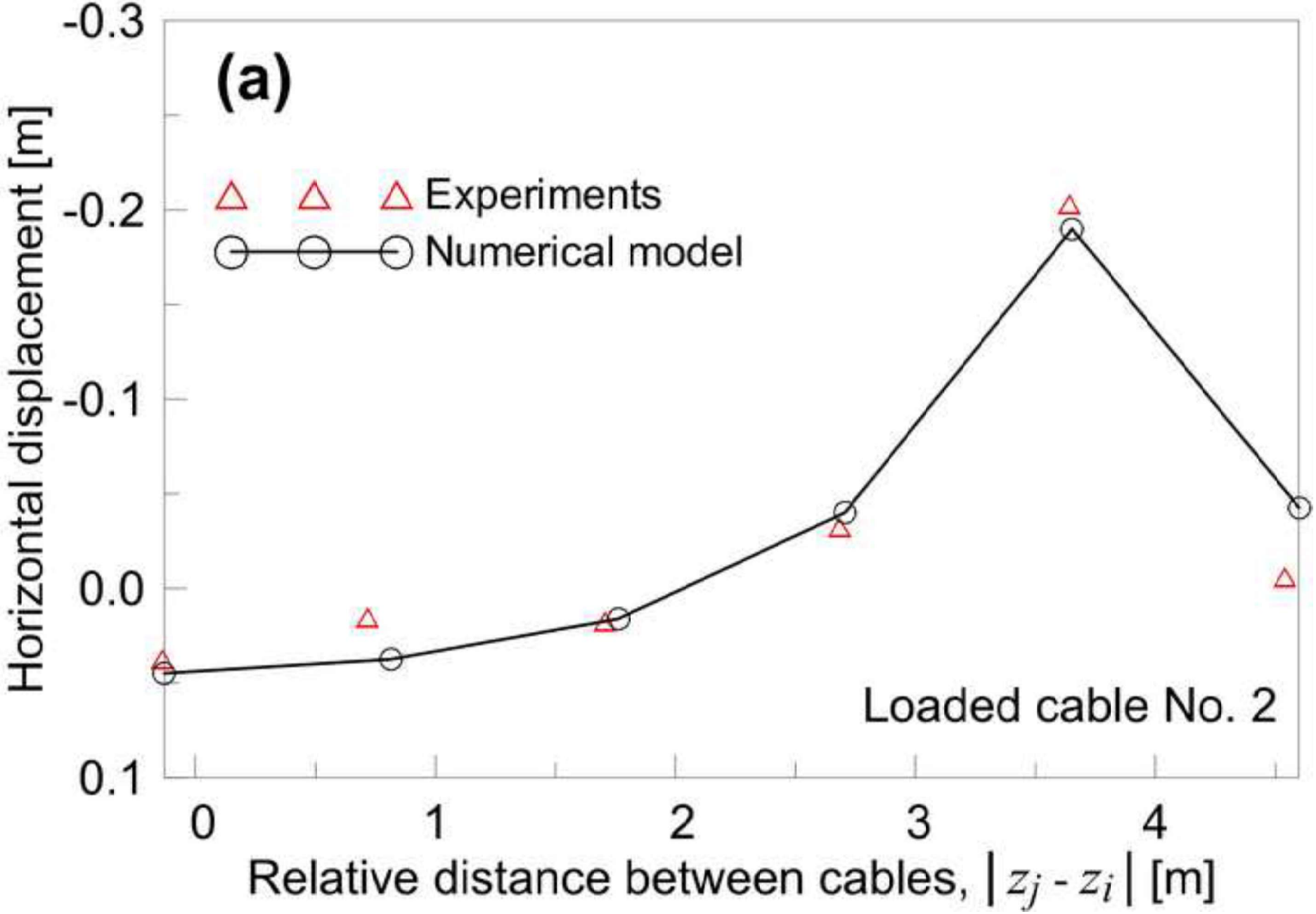

Figure 8b
Click here to download high resolution image

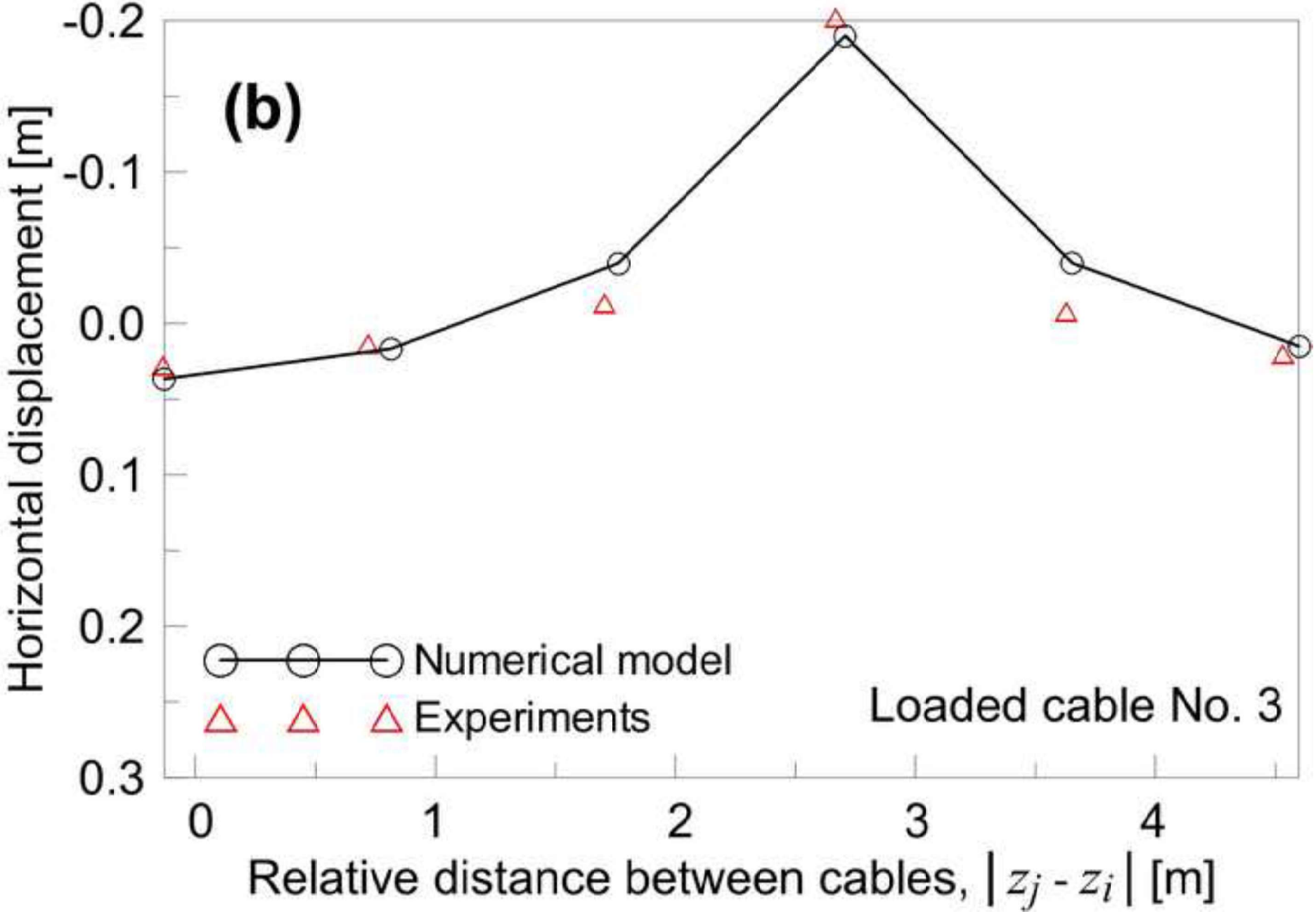

Figure 8c
Click here to download high resolution image

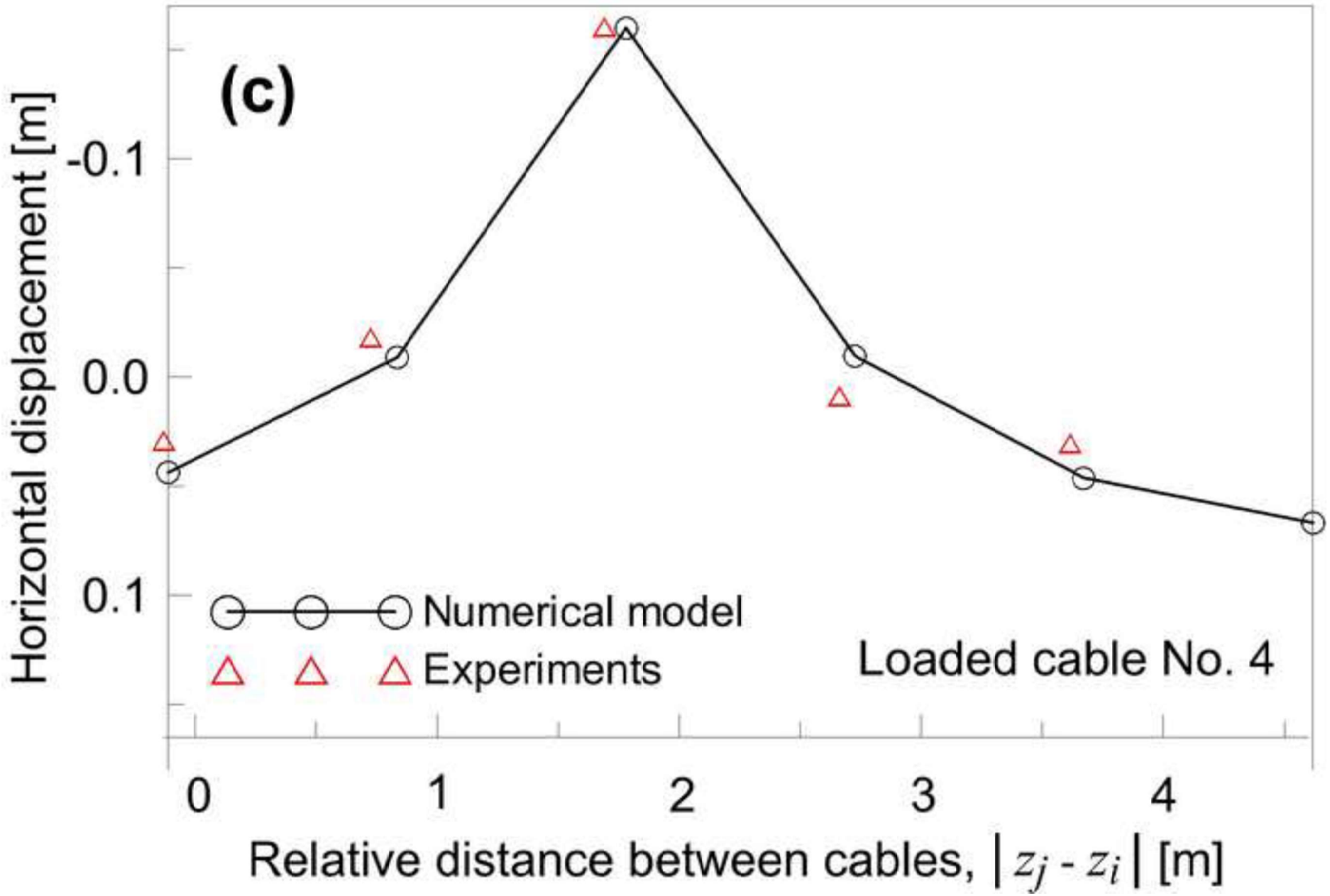

Figure 8d
Click here to download high resolution image

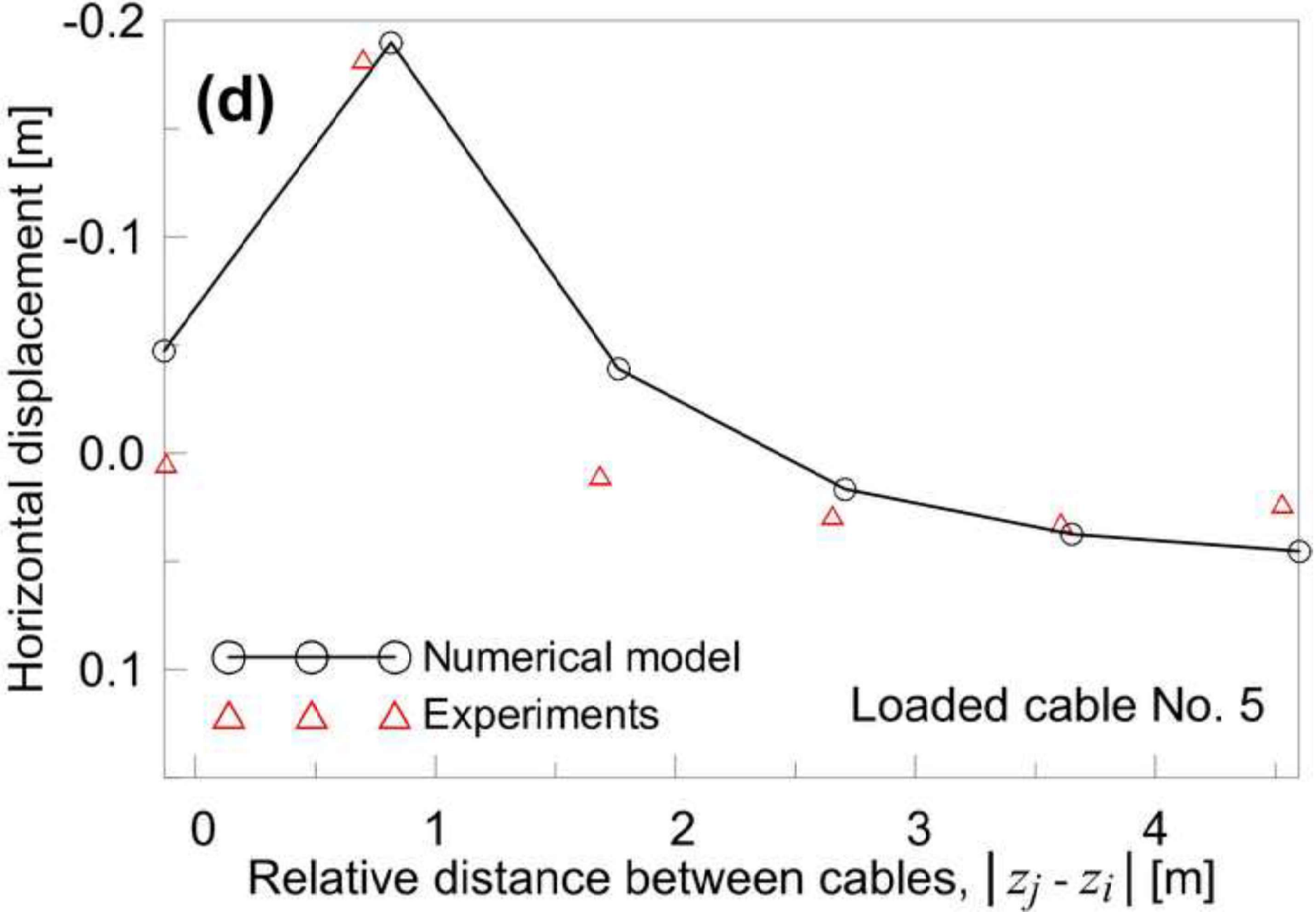

Figure 10a
Click here to download high resolution image

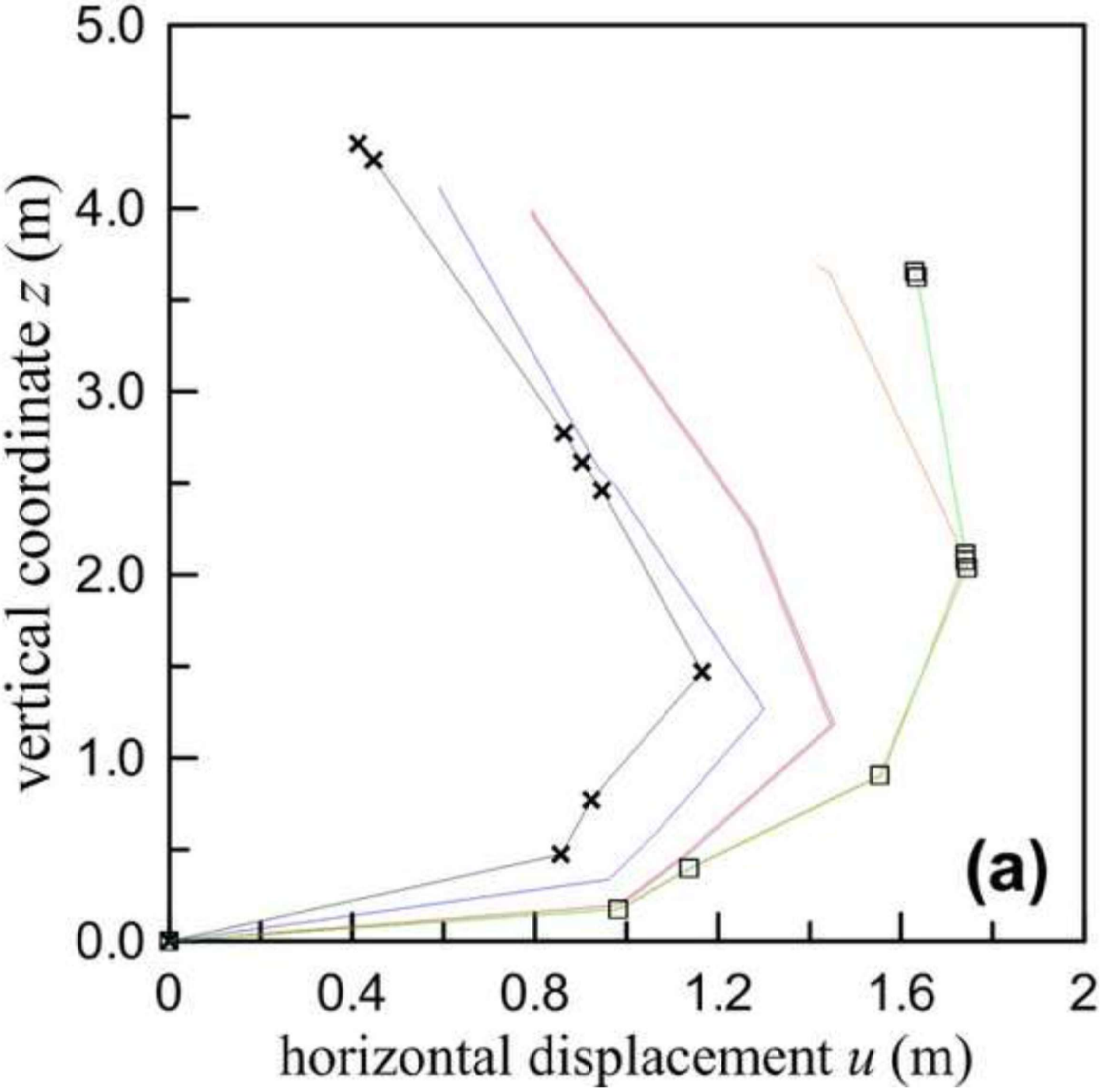

Figure 10b
Click here to download high resolution image

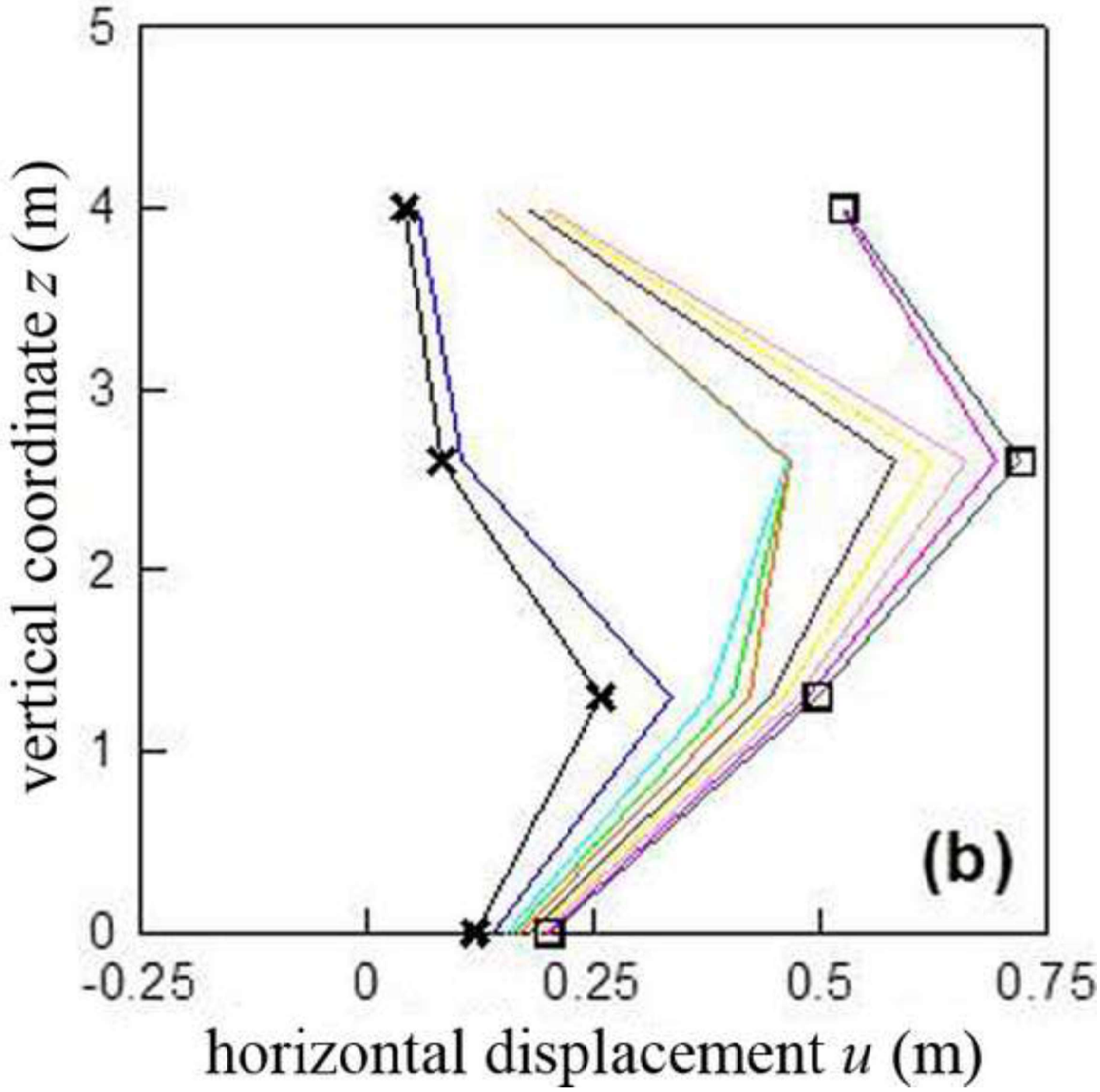

Figure 1a
Click here to download high resolution image

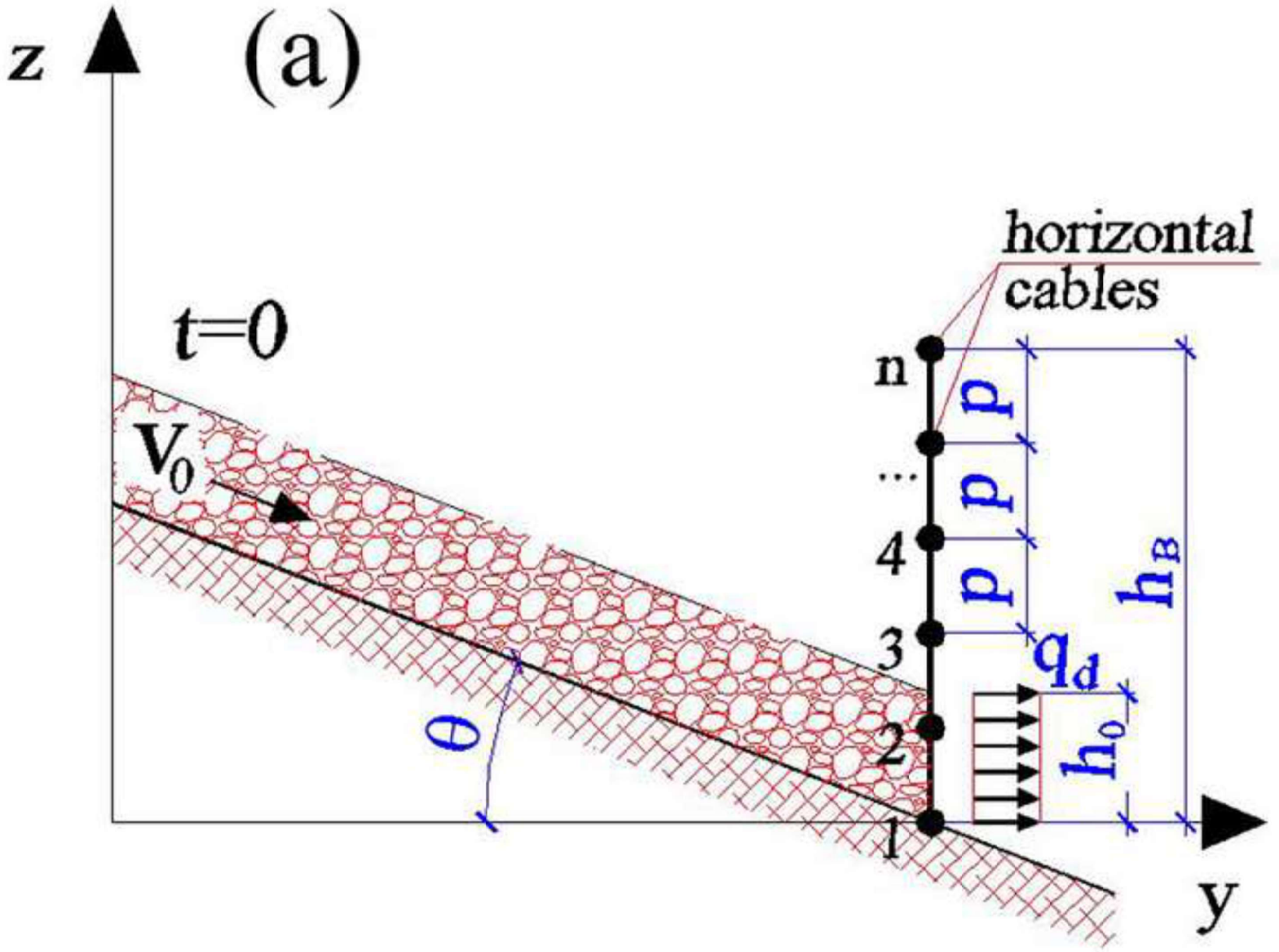

Figure 1b
Click here to download high resolution image

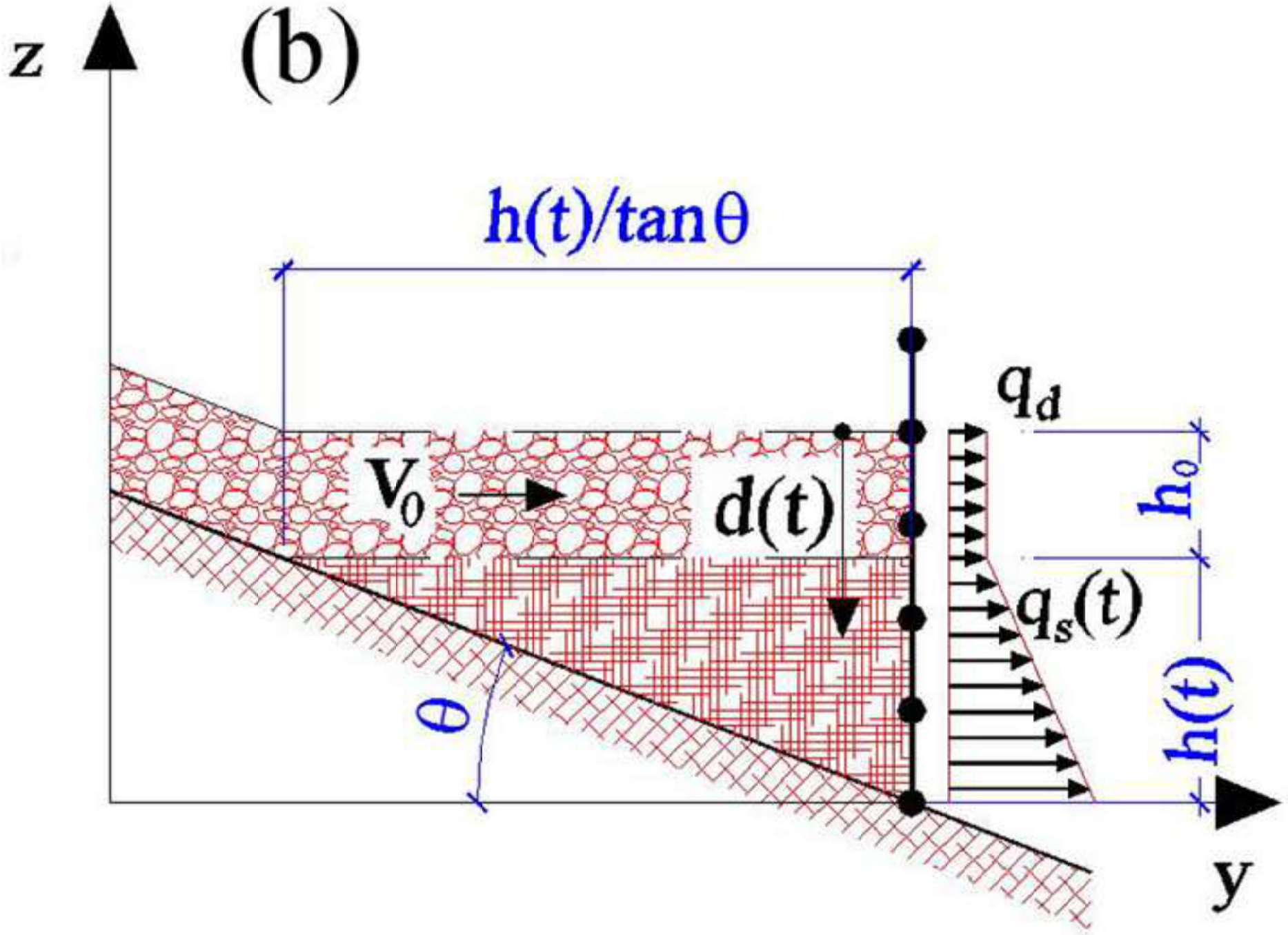

Figure 2a
Click here to download high resolution image

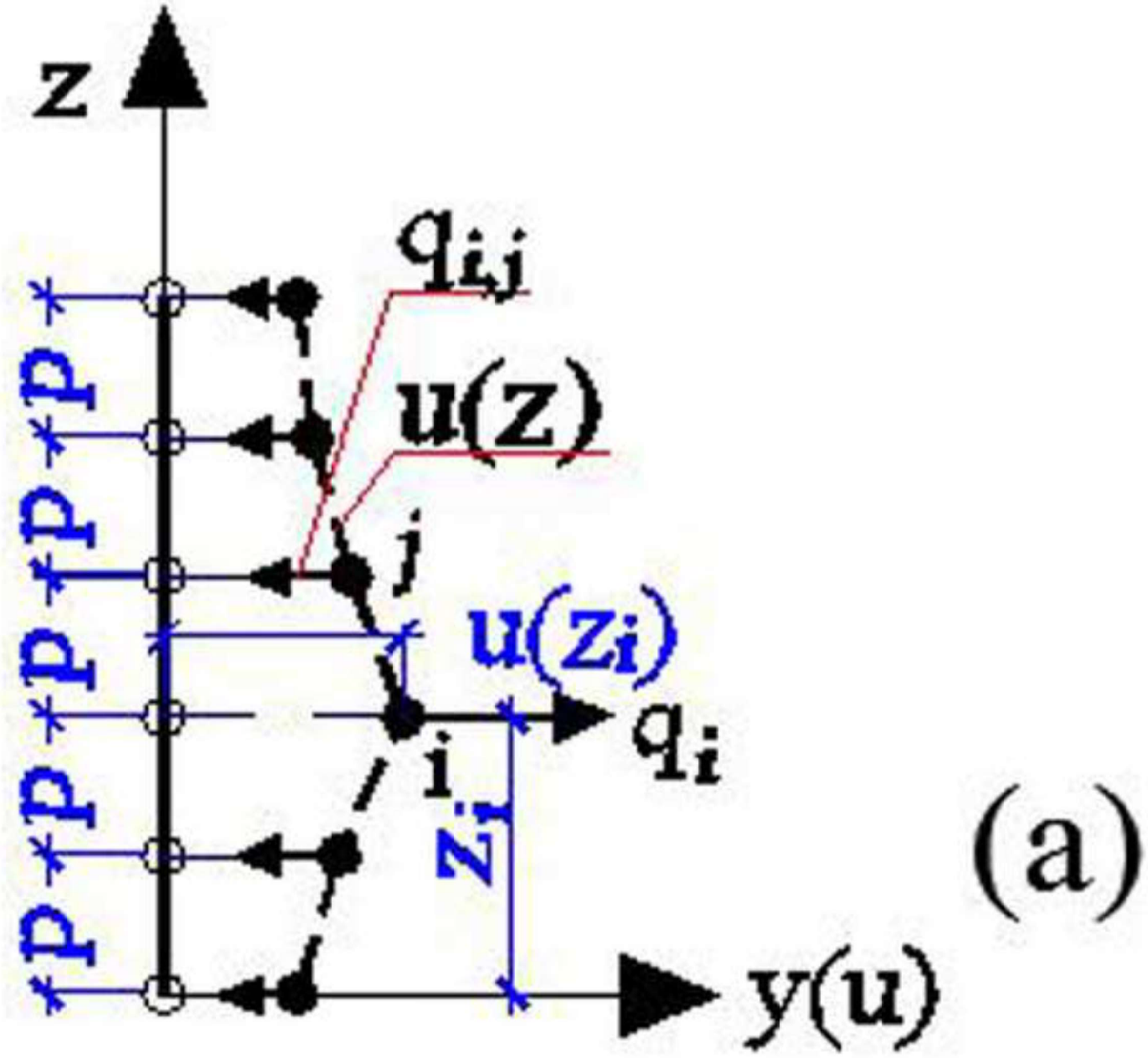

Figure 2b
Click here to download high resolution image

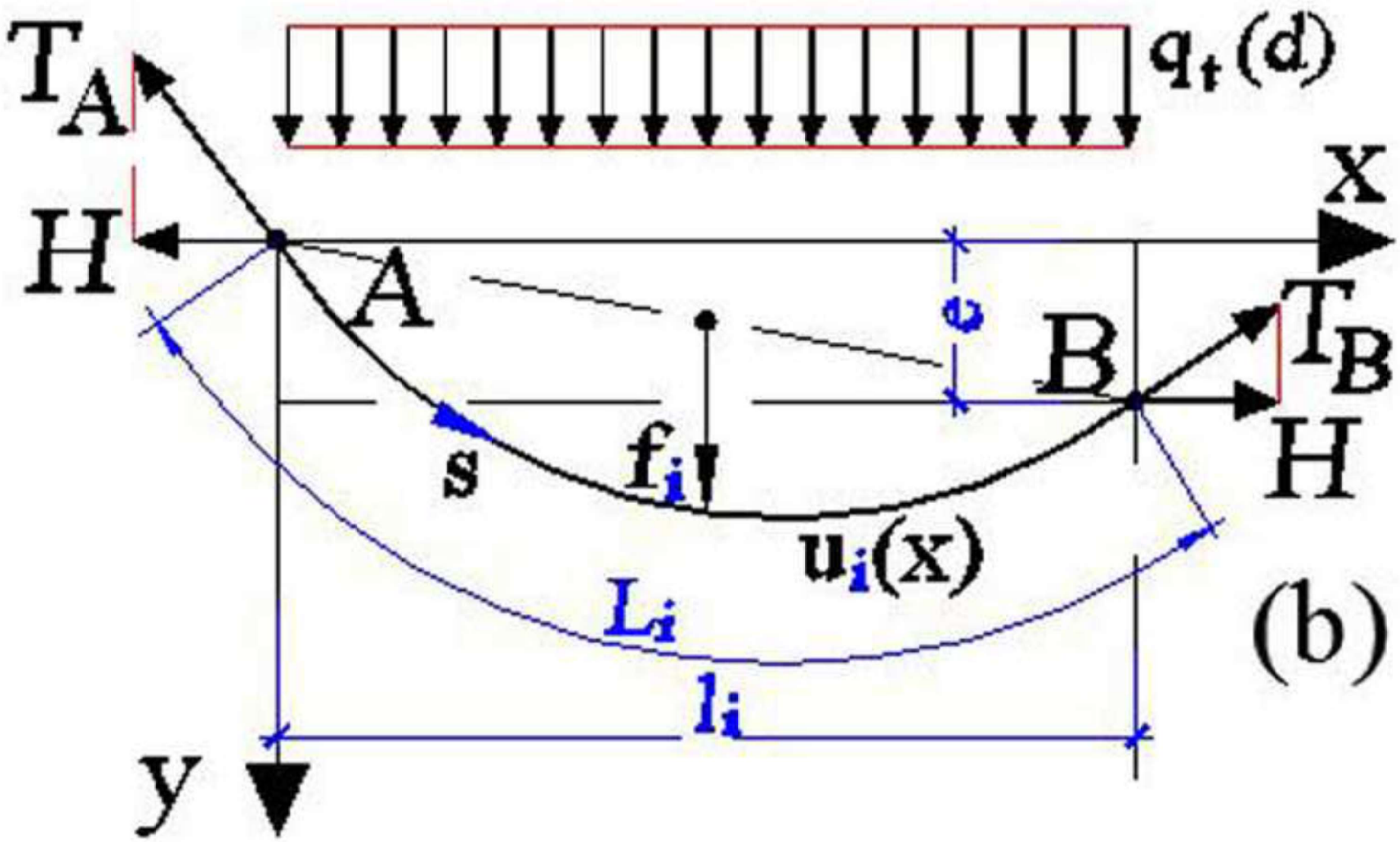

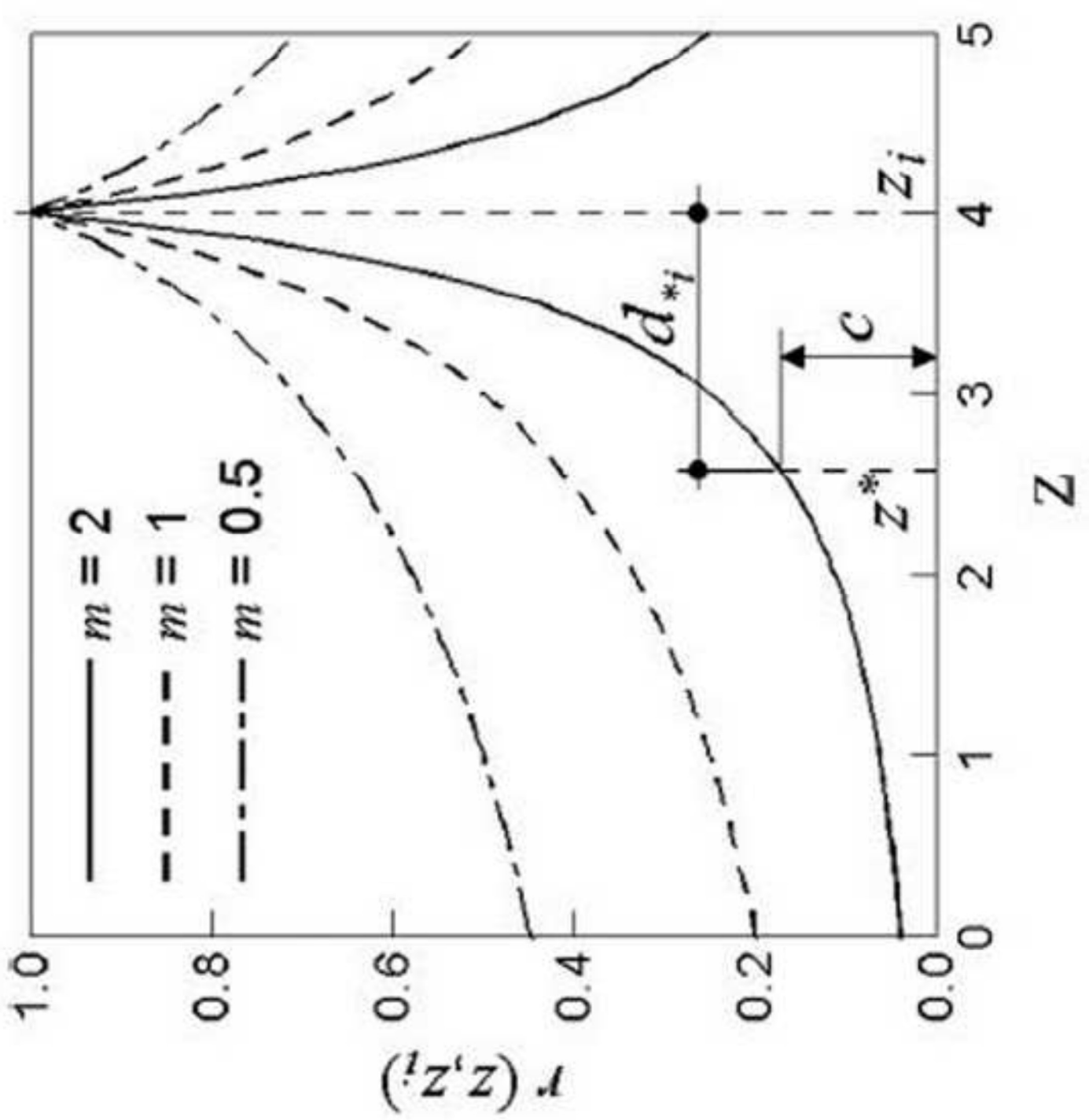

Figure 3
Click here to download high resolution image

Figure 4

Click here to download high resolution image

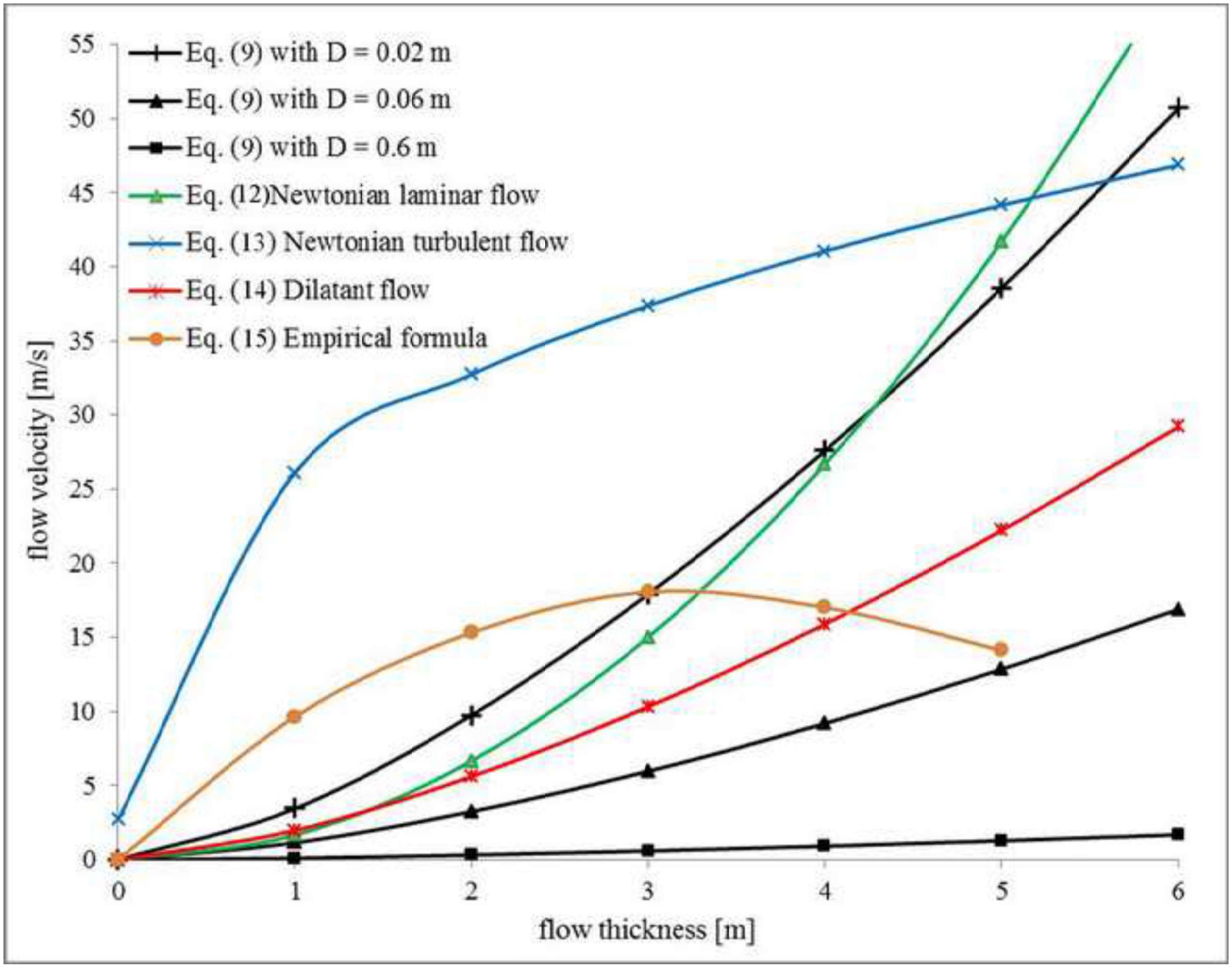

Figure 5

Click here to download high resolution image

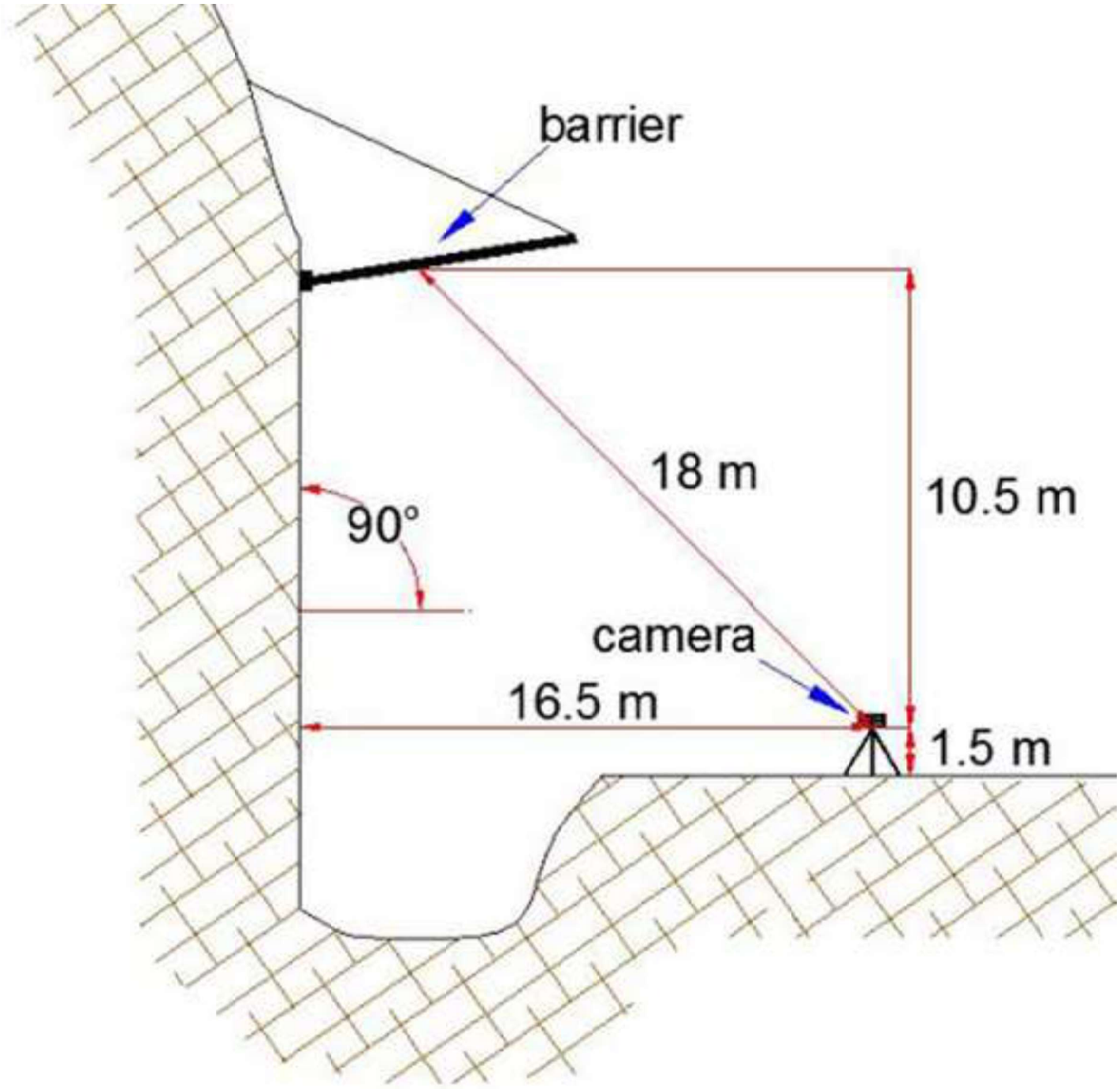

Figure 6

Click here to download high resolution image

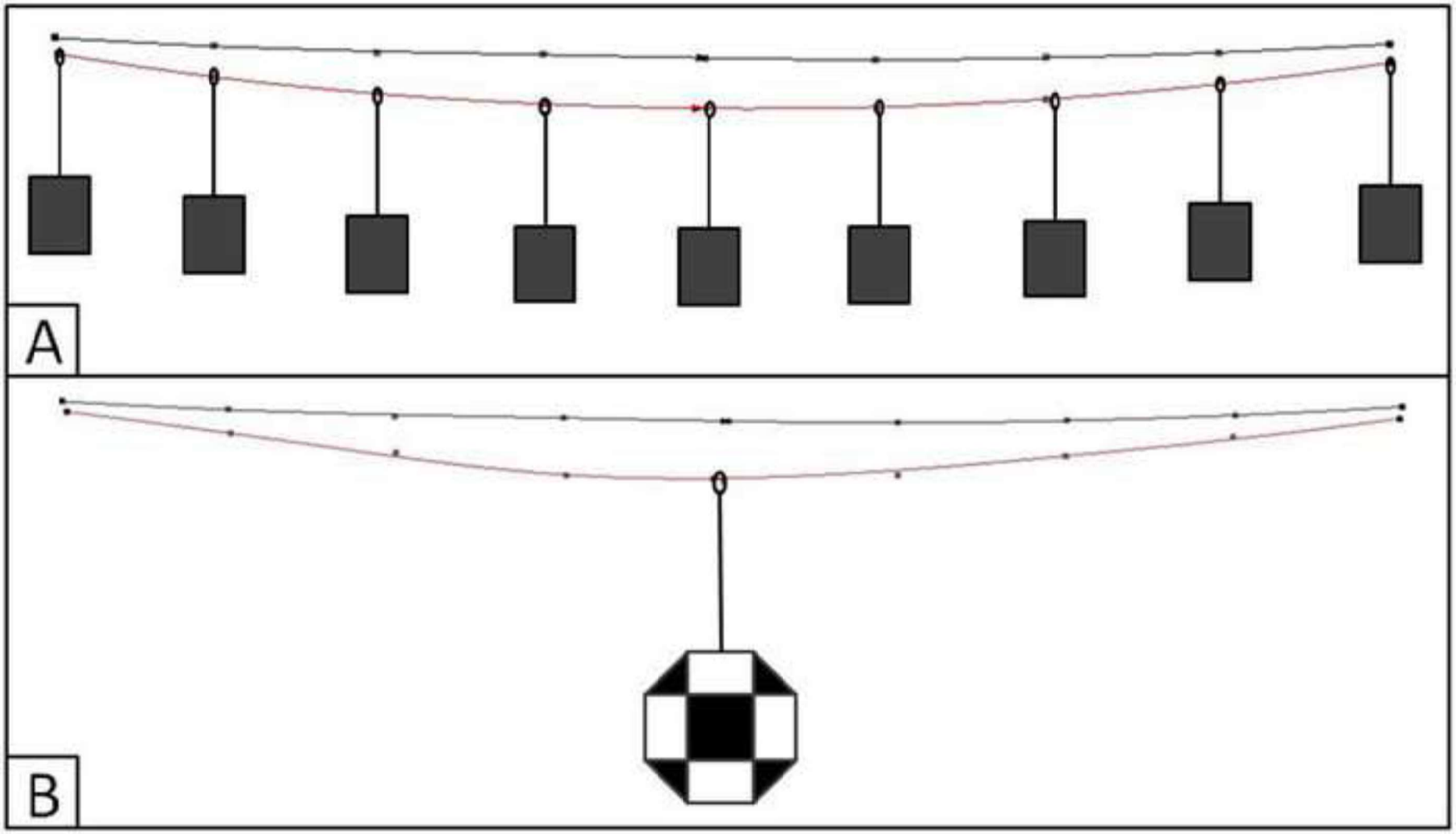

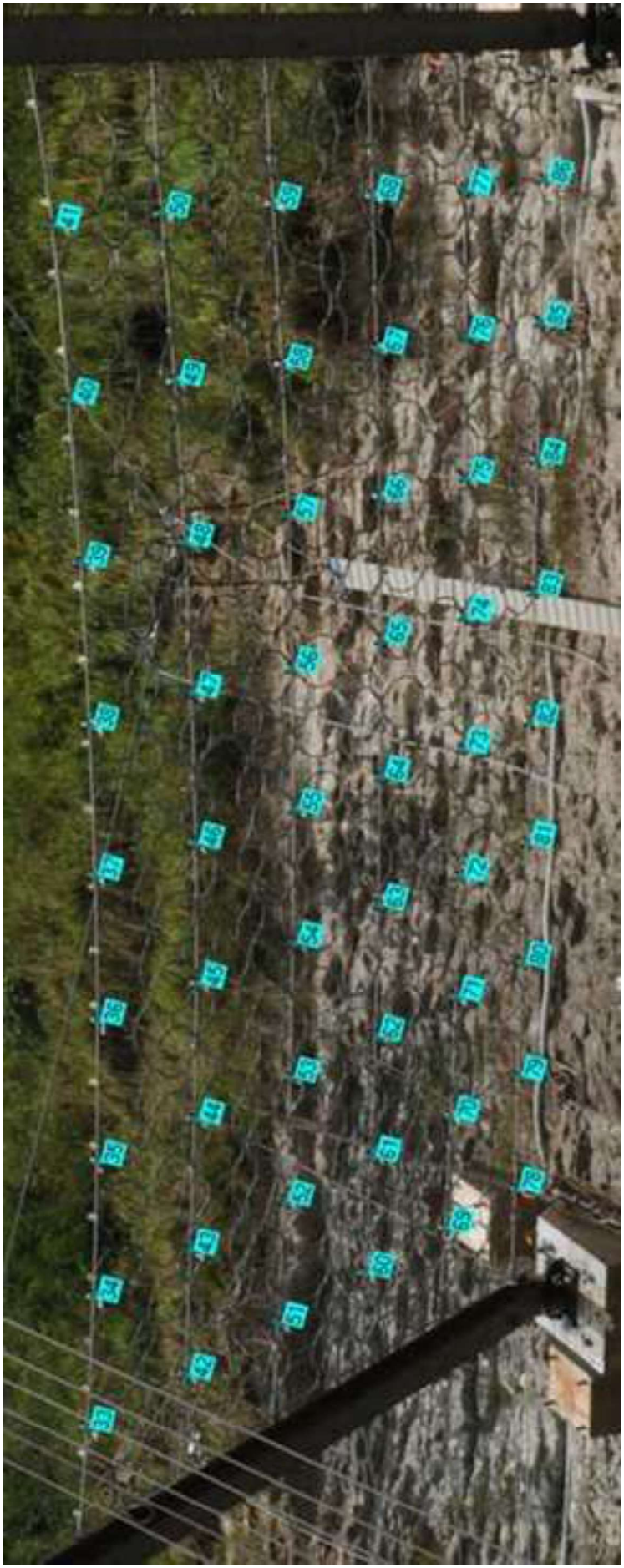

Figure 7
Click here to download high resolution image

Figure 9
Click here to download high resolution image

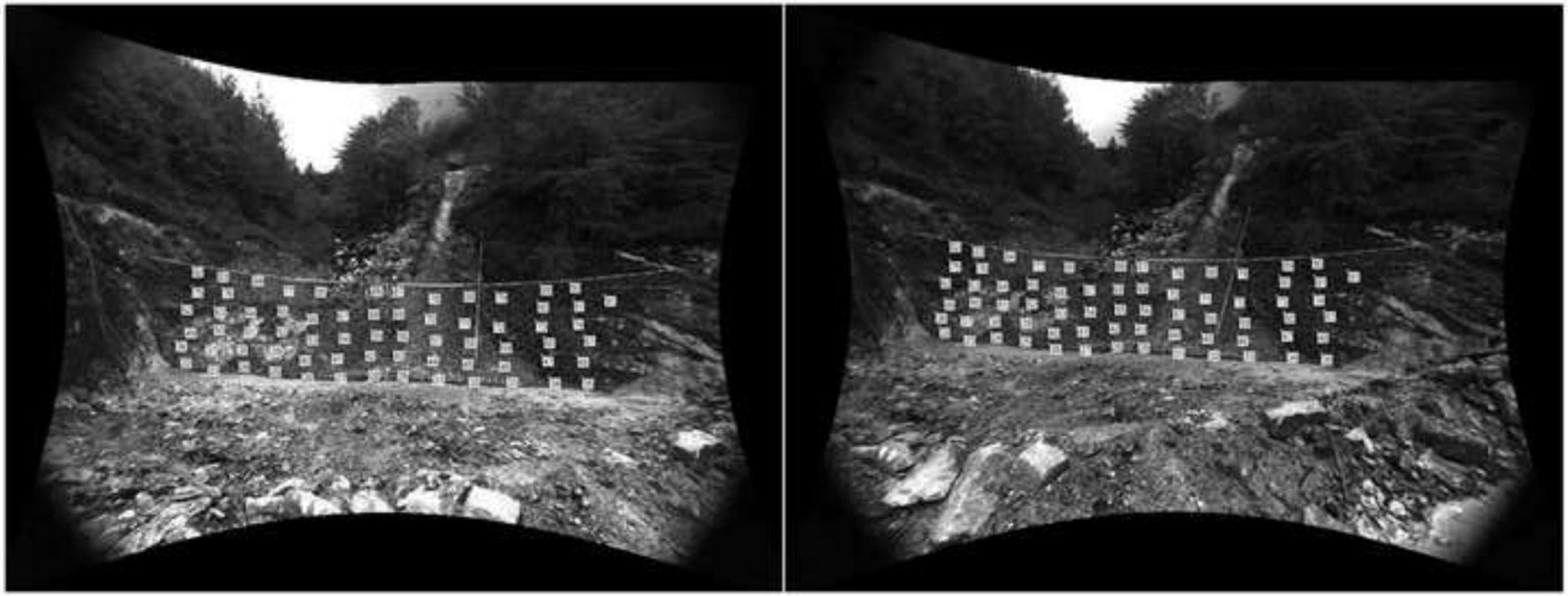

Figure 11
Click here to download high resolution image

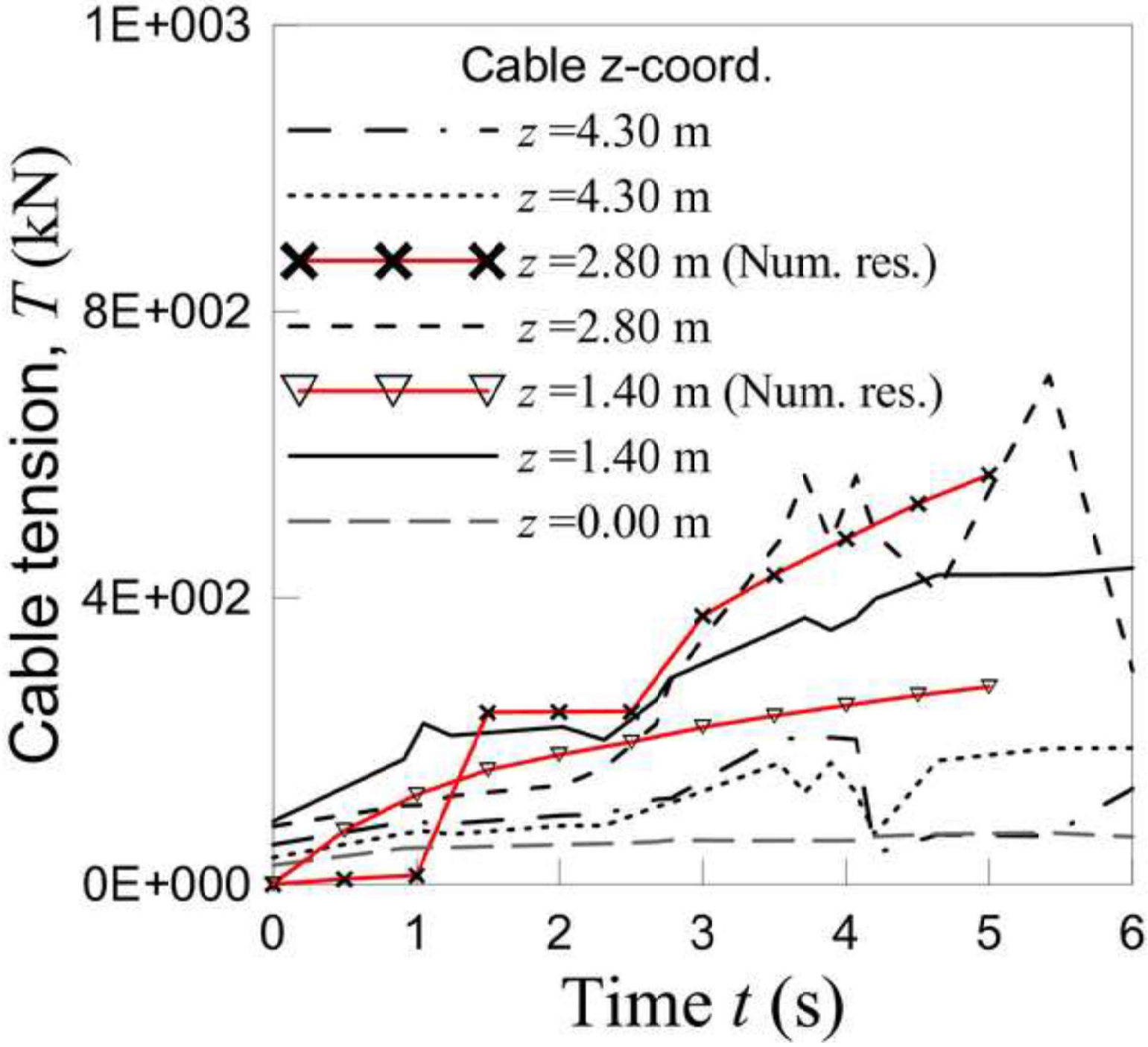

Figure 12a

Click here to download high resolution image

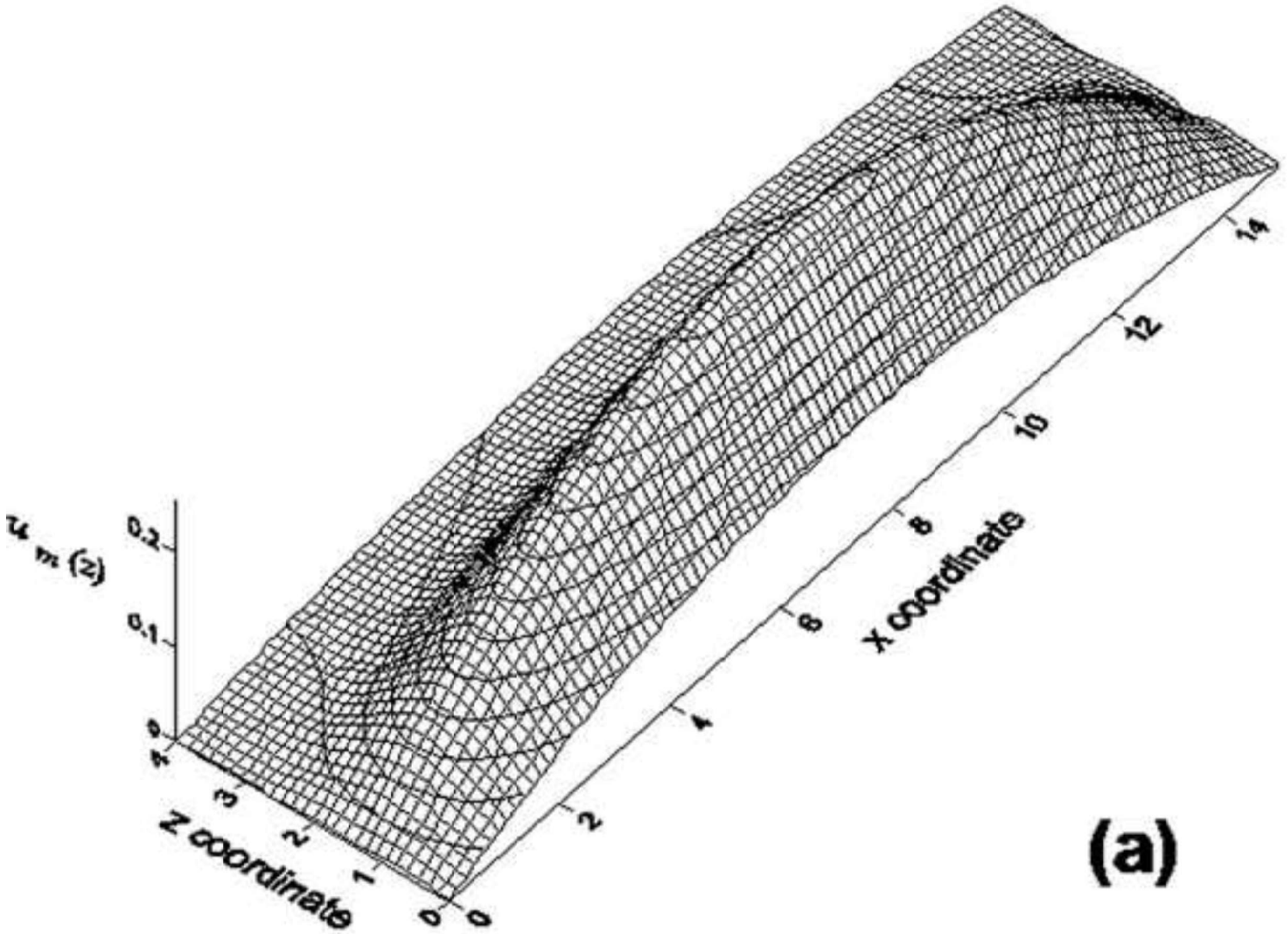

Figure 12b

Click here to download high resolution image

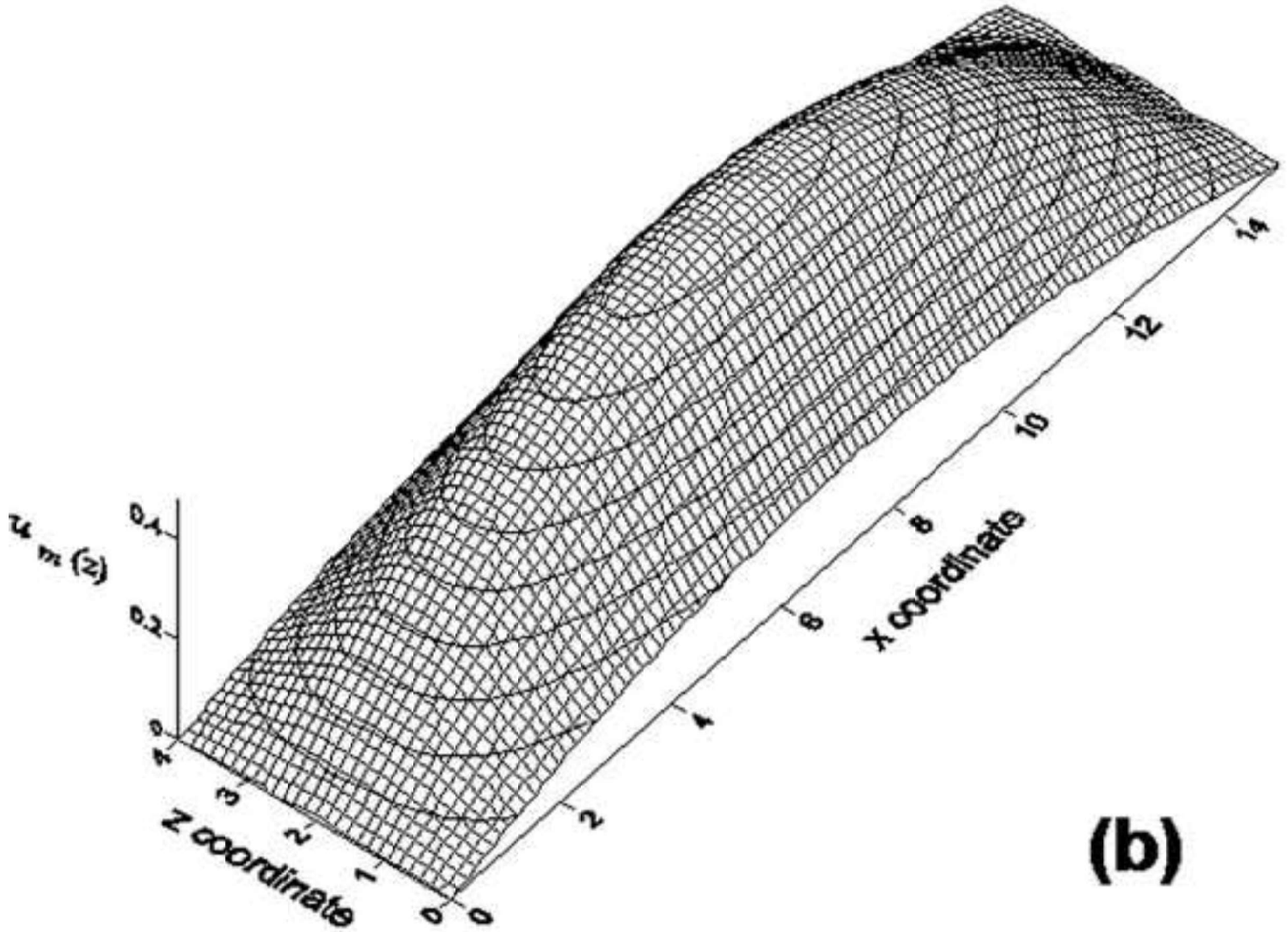

Figure 12c

Click here to download high resolution image